**ORIGINAL ARTICLE** · OPEN ACCESS

# The Diverse Habitats of Eclogite Formation: Insights From the Mesoproterozoic Glenelg Inlier, Scotland

Nicholas A. Lucas[1] 🔟 | Owen M. Weller[1] | Alex Copley[2] | Catherine M. Mottram[3] | Glenn Chapman[3] | William J. McMahon[1]

[1]Department of Earth Sciences, University of Cambridge, Cambridge, UK | [2]COMET, Department of Earth Sciences, University of Cambridge, Cambridge, UK | [3]School of the Environment, Geography and Geoscience, University of Portsmouth, Portsmouth, UK

**Correspondence:** Nicholas A. Lucas (nl423@cam.ac.uk)

**ABSTRACT**

Eclogite-facies rocks provide important constraints on the behaviour of convergent plate boundaries and the geometries of tectonic reconstructions due to the high to ultrahigh pressure conditions at which they form. Many eclogite occurrences are documented near the suture zone of active collisional settings where they are interpreted to mark the approximate location of former ocean basin subduction. Such observations influence tectonic interpretations for older eclogites within more deeply eroded and/or less well-exposed terranes. The eclogitic Glenelg inlier in northwest Scotland is one such example, with c. 1 Ga eclogites having previously been interpreted as marking the trace of a Grenville-aged collisional suture zone that defines a third 'arm' to the Grenville orogen alongside well-defined sutures in North America and Scandinavia. Here we use a combination of geochronology, phase equilibrium modelling and accessory-phase thermometry to show that the eclogite-facies assemblages were produced at ~18–19 kbar and 700°C–750°C from c. 1.1 to 1.0 Ga. Accounting for the foreland basin setting of equivalent-aged sedimentary rocks in the region and demonstrating the thermal viability of this setting, we show that eclogite formation occurred in deforming foreland crust adjacent to the Grenville orogen, in a setting broadly analogous to fault-bounded basement uplifts in the forelands of active deformation belts, such as the Himalayas and Andes. Our results demonstrate that eclogite-facies rocks can form in a greater range of tectonic settings than are sometimes considered, with implications for tectonic reconstructions of collisional zones. In this instance, our results remove the need for a third 'arm' of the Grenville orogen by placing Glenelg in a foreland setting, reconciling the absence of plentiful Grenville-aged metamorphic rocks in northwest Scotland, the sedimentological record and paleomagnetic data in the wider region.

## 1 | Introduction

Eclogite-facies rocks play a large role in tectonic reconstructions (e.g., Kellett et al. 2018), but their interpretation is fraught with difficulties. For example, estimating pressure ($P$) and temperature ($T$) conditions is hampered by the inherently high-variance assemblages that form in mafic rocks in the eclogite facies and the tendency for felsic rocks to either undergo retrograde equilibration or retain prograde assemblages through the eclogite

facies (Peterman, Hacker, and Baxter 2009; Palin et al. 2017). Progress has been made in estimating $P$–$T$ conditions using conventional thermobarometric techniques supplemented by recent advances in phase equilibrium modelling and single-element thermometers and barometers (e.g., Spear, Pattison, and Cheney 2017; Johnson, Cottle, and Larson 2021). However, the issue then becomes one of interpreting the resulting information from the perspective of the tectonic environment in which the eclogites formed. Eclogites are often found near suture zones in

collisional belts and are commonly interpreted to represent the location of ocean basin subduction and subsequent continent-continent collision (Ernst 1973; Miyashiro 1973). However, the broad *P–T* range spanned by the eclogite stability field can also include other tectonic settings, such as the deep crust and lithospheric mantle in regions of low geothermal gradients, and underthrusting continental material on the margins of distributed deformation belts. It is therefore necessary to consider multiple lines of evidence when interpreting the tectonic environment in which an eclogite-facies rock formed.

In this paper, we demonstrate this concept by interpreting the petrogenesis of eclogite-facies rocks in the c. 1 Ga Glenelg inlier, northwest Scotland. These rocks have previously been interpreted as marking a collisional suture zone, or generally the interior, of the Grenville orogen (Sanders, van Calsteren, and Hawkesworth 1984; Storey, Brewer, and Temperley 2005; Strachan et al. 2020), which was a Himalayan-scale continent–continent collisional orogen that contributed to the formation of the supercontinent Rodinia at 1090–980 Ma (Rivers 1997; Rivers et al. 2012). In this study, we combine petrology, phase equilibrium modelling, U-Pb geochronology, sedimentology and stratigraphy to interpret the provenance of the Glenelg eclogites. Our results suggest that the eclogites formed in the foreland of the Grenville orogenic belt in a setting broadly analogous to the basement-cored uplifts visible in the forelands of present-day mountain belts. Our results provide an example of using the sedimentary record at the time of metamorphism to interpret the provenance of eclogite-facies rocks. The results imply a new interpretation of the geometry of the Grenville orogen with respect to the British Isles and showcase the diverse tectonic settings in which eclogites can form.

We first describe the geological context and previous work on the Glenelg inlier. Next, we describe the petrography of mafic eclogite and felsic garnet-omphacite gneiss (hereafter 'felsic gneiss') samples from the inlier and provide refined constraints on the age and *P–T* conditions of metamorphism. We then discuss the distribution, architecture, age and depositional setting of Grenville-aged sedimentary rocks in the region and the constraints these data place on the provenance of the eclogites. Finally, we combine these diverse sources of information into a coherent model for the formation of the Glenelg eclogite, demonstrate the thermal viability of this model and discuss the wider implications of our results.

## 2 | Geological Context and Previous Work

The Glenelg inlier of northwest Scotland is one of the few indicators of Grenville-aged (c. 1.2–1.0 Ga) metamorphism and deformation in the British Isles (Sanders, van Calsteren, and Hawkesworth 1984; Storey 2008), in contrast to the spatially widespread record of metamorphism and deformation in North America and Scandinavia (Weller et al. 2021). The inlier is also the only eclogite-facies locality in the British Isles (Storey 2008).

The c. 1.2–1.0 Ga Grenville orogen includes an early accretionary phase initiated at c. 1190 Ma (in its type locality in Canada Rivers 1997; Rivers et al. 2012), followed by a continent–continent

collisional event (1090–985 Ma) between the Amazonian craton (in South America) and the Laurentian and Baltican cratons (in North America and Scandinavia, respectively), ultimately leading to the assembly of the supercontinent Rodinia (Hoffman 1991; Rivers 1997; Rivers et al. 2012). In North America, the orogen is thought to have attained double-thickness crust (70-80 km) at 1090–1050 Ma, with granulite facies conditions of 8–11 kbar and 800°C–900°C characterising the middle crust (Rivers et al. 2012). Metamorphosed and deformed rocks associated with the orogen outcrop over a distance of over 2000 km (Rivers 1997; Rivers et al. 2012). The Grenville orogen is also well exposed in Norway and Sweden, where a contemporaneous record of regional metamorphism is preserved (locally known as the Sveconorwegian orogen; Bingen et al. 2021). The orogenic belt is also thought to pass through the British Isles based primarily upon the Glenelg eclogites having a Grenvillian age (c. 1 Ga; Sanders, van Calsteren, and Hawkesworth 1984; Brewer et al. 2003; Bird et al. 2023) and similarly aged deformation in northwest Ireland (i.e., Annagh Gneiss Complex, Figure 1; Daly 1996; Daly and Flowerdew 2005). However, evidence of Grenville-aged metamorphism and deformation in this region is otherwise lacking, making the exact geometry of the Grenville orogen in the British Isles uncertain.

### 2.1 | Structural Setting of the Glenelg Inlier

The Glenelg inlier is situated within the 'Moine' nappe in northwest Scotland, which formed during fold-thrust belt emplacement during the c. 470–420 Ma Caledonian orogeny (Searle 2022) and transported the older Grenville-aged Glenelg eclogite to its current structural setting (Figure 1; Ramsay 1957; Sutton and Watson 1958; Krabbendam et al. 2018). Northwest-to west-northwest-directed Caledonian thrusting resulted in the juxtaposition of three tectonostratigraphic units as preserved in northwest Scotland (Johnstone, Smith, and Harris 1969): the Caledonian foreland, the Moine nappe and the overlying Sgurr Beag nappe (Figure 1). The Caledonian foreland consists of Archean gneiss (known as the Lewisian Gneiss Complex) overlain by largely unmetamorphosed Neoproterozoic sandstones of the Stoer, Sleat and Torridon Groups (Peach et al. 1907; Wheeler et al. 2010). The foreland stratigraphy is locally disrupted by the Kishorn thrust and its overlying nappe (Figure 1; Sutton and Watson 1964). The Moine and Sgurr Beag nappes are composed mainly of Neoproterozoic meta-siliciclastic rocks. The Moine nappe is bound to the northwest by the Moine thrust (Peach et al. 1907) and is dominated by greenschist- to middle amphibolite-facies psammite (Kennedy 1949; Soper and Brown 1972; Fettes et al. 1985; Mazza et al. 2018). The structurally overlying Sgurr Beag nappe was emplaced along the Sgurr Beag thrust and is characterised by upper amphibolite-facies (semi)pelite and psammite (Tanner 1971; Barr, Holdsworth, and Roberts 1986; Cutts et al. 2010; Mazza et al. 2018).

The Glenelg inlier is one of several basement inliers exposed within northwest Scotland, which mainly occur within the Moine nappe (Figure 1; e.g., Peach et al. 1910). The inliers display dominantly amphibolite-facies assemblages, but relict granulite-facies assemblages are found within some localities (Fettes et al. 1985; Holdsworth, Strachan, and Alsop 2001; Holdsworth, Strachan, and Harris 1994). The inliers have been
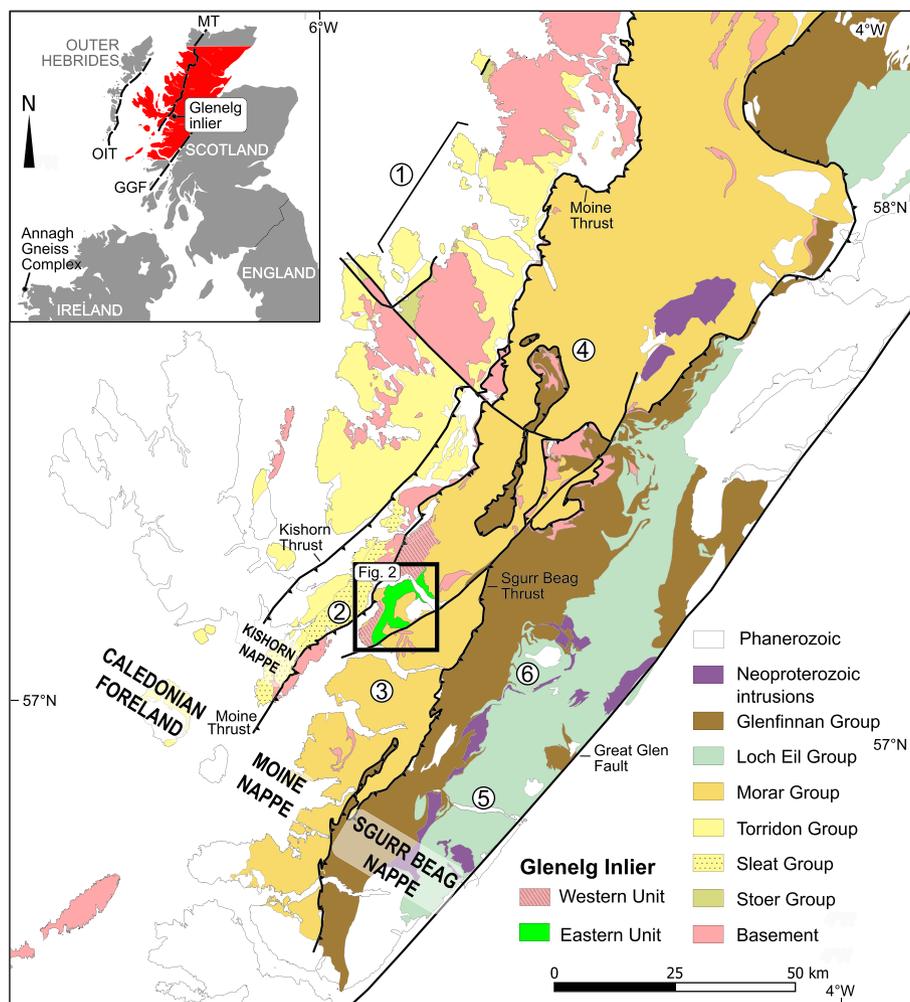
**FIGURE 1** | Simplified geological map of northwest Scotland after British Geological Survey (2007), with the geographical extent highlighted in red in the inset map. The Eastern Unit of the Glenelg inlier, hosting the Grenville-aged eclogites of focus in this study, is shown in bright green. Circled numbers correspond to the representative stratigraphic columns shown in Figure 12. GGF = Great Glen fault; MT = Moine thrust; OIT = Outer Isle thrust.

correlated with the Lewisian foreland on the basis of their common Neoarchean-Paleoproterozoic magmatic and metamorphic histories (Friend, Strachan, and Kinny 2008; Strachan et al. 2020). However, the Glenelg inlier is distinct in terms of hosting c. 1 Ga eclogites, along with typical Lewisian lithologies (Sanders, van Calsteren, and Hawkesworth 1984).

## 2.2 | The Geological History of the Glenelg Inlier

The inlier (Figure 2) consists of two juxtaposed Neoarchean crustal blocks ('Eastern Unit' and 'Western Unit') surrounded by early Neoproterozoic psammite forming the Morar Group (Storey 2008; Storey et al. 2010; Krabbendam et al. 2018). Previous studies have discussed structural fabrics within these units in detail (May et al. 1993; Storey 2008; Barber 2011; Krabbendam et al. 2018). Within the Western Unit, granulite- and eclogite-facies metamorphism is locally preserved in metabasic rocks at c. 2.8–2.6 Ga and c. 1.75 Ga, respectively (Storey et al. 2010). These relicts are embedded within widespread amphibolite-facies leucocratic orthogneiss, with an assumed Caledonian age of retrograde metamorphism (Storey 2008). The Western Unit lithologies

are in faulted contact with the Eastern Unit ('Barnhill' shear zone of Storey 2002; Figure 2) and are not investigated in this study as they only record pre-Grenvillian high pressure metamorphism.

In contrast, the Eastern Unit exposes abundant mafic eclogite (up to 25% of the outcrop) alongside felsic gneiss, marble, (semi)pelitic schist and gneiss and ultramafic rocks (Figure 2; Rawson, Carswell, and Smallwood 2001; Storey 2008). Eastern Unit felsic gneiss forms the oldest component with a protolith age of c. 2.8 Ga (Storey 2002). The mafic eclogite has a protolith age of c. 2.1 Ga (Brewer et al. 2003). An oceanic origin has been suggested for these units based on the eclogite's MORB-like major and trace element signature (Storey 2002). However, such signatures may be modified during metamorphism (e.g., Zhao et al. 2007), particularly in the case of the Glenelg eclogites, where multiple mountain-building events are recorded (i.e., the Grenville- and Caledonian-aged orogenies). Furthermore, regardless of the eclogite's origin, the ~1 Ga time gap between protolith formation and Grenville-aged metamorphism means that the material must have been incorporated into continental crust at some point prior to eclogite-facies metamorphism. This inference is based upon the much shorter timescale (<200
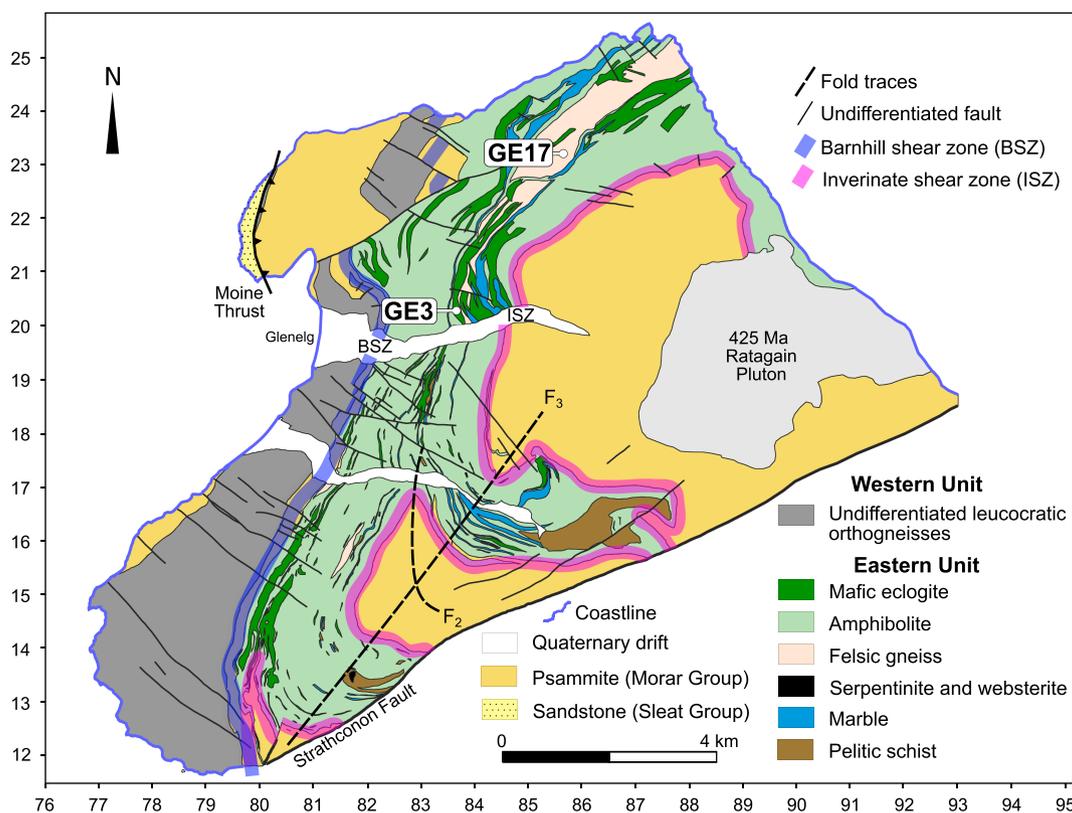
**FIGURE 2** | Geological map of the main Glenelg inlier exposure modified from Storey (2008), showing the locations of the two study samples (GE3 and GE17). Coordinate system: British National Grid, area 'NG'.

Myr) of recycling of oceanic lithosphere into the mantle by subduction, with only continental crust able to have a billion-year lifespan at the Earth's surface. The mafic eclogites are typified by the assemblage omphacite-garnet-quartz-rutile± amphibole, and are cross-cut by amphibolite-facies retrogression fronts. The felsic gneiss is characterised by the assemblage omphacite-garnet-plagioclase-kyanite-quartz-rutile.

Reported metamorphic age estimates from the Glenelg eclogites vary between c. 1.2 and 0.9 Ga. Sanders, van Calsteren, and Hawkesworth (1984) obtained Sm-Nd garnet-clinopyroxene-whole-rock isochron ages of $1082 \pm 24$ and $1010 \pm 13$ Ma, which they interpreted as recording peak and retrograde conditions, respectively. Brewer et al. (2003) obtained a U-Pb zircon age of $995 \pm 8$ Ma and U-Pb titanite age of $971 \pm 65$ Ma, which they interpreted as recording retrograde conditions based on textural criteria. Bird et al. (2023) obtained Lu-Hf garnet-whole-rock isochron ages of 1218–1137 Ma (mafic eclogite) and 1162–1040 Ma (garnet- and kyanite-bearing metapelite) and Sm-Nd garnet-whole-rock ages of 1007–809 Ma (eclogite) and 948–903 Ma (metapelite). They interpreted the Lu-Hf ages as representing garnet core-to-rim growth, thus placing an upper age limit on peak metamorphic conditions, and the Sm-Nd ages as representing cooling during exhumation. Collectively, these data suggest peak eclogite-facies conditions that occurred around c. 1.1 to 1.0 Ga.

Several studies have analysed the *P–T* history of Glenelg, primarily using conventional thermobarometric techniques. Sanders (1988) and Manning and Bohlen (1991) obtained similar estimates of 16–17 kbar and 740°C–750°C from a felsic gneiss sample, which Sanders (1988) interpreted as minimum

peak metamorphic conditions based on petrographic criteria. Rawson, Carswell, and Smallwood (2001) and Storey, Brewer, and Temperley (2005) obtained similar estimates of 20 kbar and 730°C–780°C from a garnet-bearing olivine–websterite and felsic gneiss, which they interpreted as peak metamorphic conditions. Storey, Brewer, and Temperley (2005) also obtained estimates of 13–15 kbar and 650°C–700°C from symplectite colonies in both felsic gneiss and mafic eclogite samples, which they interpreted as recording retrograde metamorphism based on the analysed microstructural setting. Sajeev et al. (2010) obtained estimates of 22 kbar and 670°C, 18 kbar and 850°C and 25 kbar and 1000°C from mafic eclogite samples distributed across the inlier, which they interpreted as recording geologically varied peak-metamorphic conditions.

The Eastern Unit occurs in faulted contact with the Morar Group psammite ('Inverinate' shear zone of Storey 2002; Figure 2). The final emplacement of the Eastern Unit occurred during Caledonian-aged deformation (c. 437–415 Ma Storey 2002; Storey, Brewer, and Parrish 2004; Searle 2022).

## 3 | Petrography and Mineral Chemistry

We collected a suite of samples from the Eastern Unit, of which two samples of contrasting bulk composition were selected for detailed analysis (Figure 2): mafic eclogite sample GE3 (−5.58534°W, 57.22233°N; British National Grid: NG 83650 20318) and felsic gneiss sample GE17 (−5.55073°W, 57.25061°N; NG 85902 23355).

## 3.1 | Methods

Major element mineral analyses were acquired using a Cameca SX-100 electron probe micro-analyser (EPMA) at the University of Cambridge. The accelerating voltage was 20 kV and beam current 20 nA, with a beam size of 1 to 5 μm and 10 to 60 s dwell times. Natural standards were used for calibration, and a ZAF correction procedure was used. The programme AX (version Oct-2019 Holland 2009) was used for mineral cation calculation, which provides an estimate of $Fe^{3+}$ cations per formula unit (cpfu) where applicable based on stoichiometric criteria. Mineral abbreviations follow the guidelines of Whitney and Evans (2010). Mineral modes were obtained by Quantitative Evaluation of Minerals by Scanning Electron Microscopy (QEMSCAN), using an FEI Quanta 650F Scanning Electron Microscope, also at the University of Cambridge.

## 3.2 | Mafic Eclogite (GE3)

Sample GE3 features a granular texture defined primarily by garnet (41 vol.%) and omphacite (38 vol.%), in addition to quartz (9 vol.%), calcic amphibole (6 vol.%), plagioclase (4 vol.%) and accessory rutile, titanite, apatite, ilmenite, epidote, K-feldspar, biotite, magnetite, iron sulphides, zircon and muscovite (Figure 3a).

Garnet forms anhedral grains up to ~3 mm in diameter and is commonly surrounded by thin and discontinuous plagioclase coronae (Figure 3a,b). Garnet chemistry features a compositionally homogeneous core ($Alm_{47}Prp_{33}Grs_{19}Sps_1$) and a zoned mantle featuring a rimward increase in grossular and coupled decrease in almandine and pyrope content towards an inner rim plateau ($Alm_{44}Prp_{30}Grs_{25}Sps_1$). Thin garnet rims feature deflections in grossular, almandine and pyrope content, which vary between grains (Figure 4). Inclusions are common throughout the grains and include quartz, omphacite, rutile and apatite. Omphacite is up to ~1 mm across, with diopside-plagioclase-amphibole symplectites occurring along some grain boundaries (Figure 3d). Omphacite grain interiors exhibit uniform compositions ($Di_{56}Jd_{25}Hed_{12}Aeg_7$), with grain rims more diopside rich. Omphacite inclusions mainly consist of quartz, rutile and apatite. Quartz also occurs as blebs throughout the matrix (Figure 3a).

Amphibole occurs in two distinct settings: as platy grains in the matrix up to ~1 mm long and as <20 μm of grains within diopside-plagioclase-amphibole symplectites along omphacite
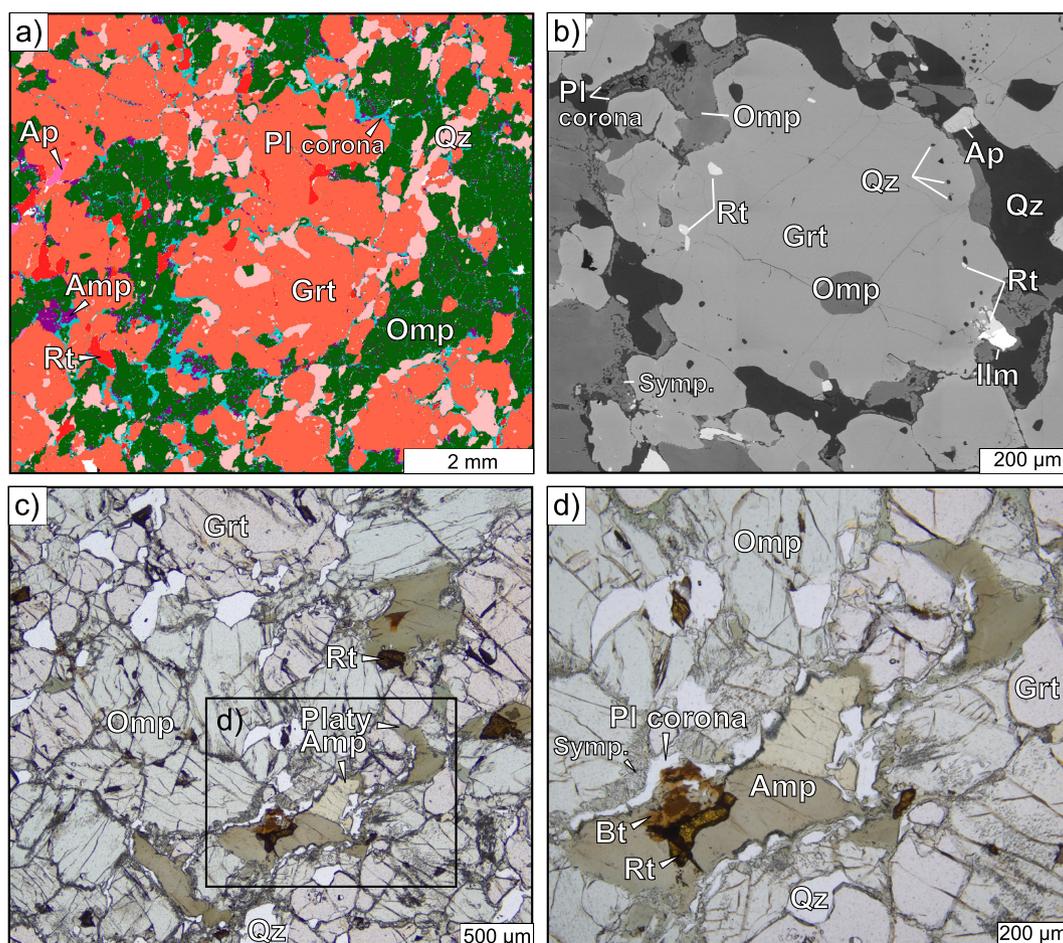


**FIGURE 3** | Mafic eclogite sample GE3 petrography. (a) QEMSCAN phase map showing a coarse-grained granular texture defined mainly by garnet and omphacite. (b) Resorbed garnet porphyroblast containing inclusions of omphacite, quartz and rutile. (c) Plane-polarised light photomicrograph displaying a granular microstructure defined by garnet, omphacite, quartz and platy amphibole. (d) Close up of the area demarcated in (c) showing ragged biotite grains adjacent to rutile, plagioclase coronae around platy amphibole and fine-grained symplectite colonies invading omphacite grain boundaries.
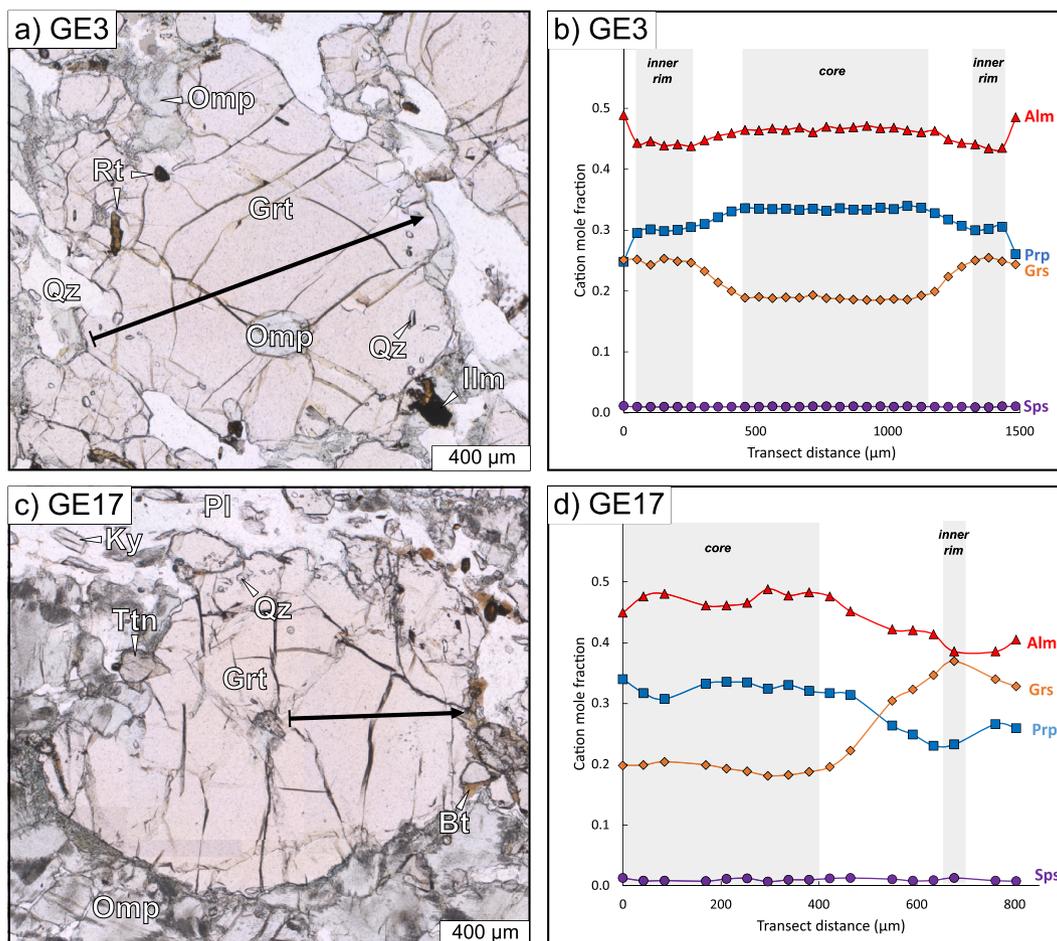
**FIGURE 4** | (a) Plane-polarised light photomicrograph showing the location of the compositional transect across a garnet grain provided in (b) for mafic eclogite sample GE3. (c, d) As in (a) and (b) but for felsic gneiss sample GE17.

grain boundaries (Figure 3c,d). The platy grains generally exhibit straight grain boundaries where in contact with omphacite and garnet, and ragged grain boundaries where in contact with coronitic plagioclase (Figure 3c,d). Platy amphibole contains rutile inclusions and in places appears to be replaced by ragged biotite (Figures 3d and S1). Platy amphibole is pargasitic and features a high-Na core (up to 0.34 $Na_B$ pfu) and low-Na rim (0.10−0.20 $Na_B$ pfu) (Figure S1c). Symplectite amphibole is pargasite to edenite-hornblende in composition and has 0.04−0.14 $Na_B$ pfu (Figure S1a).

Plagioclase occurs as coronae around some garnet and platy amphibole grains and as part of symplectite colonies invading omphacite grain boundaries (Figure 3a,d). Plagioclase in both settings is dominantly oligoclase in composition ($X_{Ab}$ = 0.74-0.86). Rutile is up to ∼0.5 mm, features an irregular to euhedral habit and occurs as inclusions and matrix grains (Figure 3c,d). Ilmenite occurs both as lamellae within rutile, and as grains partially replacing rutile. Titanite also occurs as micron-scale coronae around some rutile grains. Epidote, K-feldspar, biotite and muscovite are volumetrically minor phases and are concentrated along fractures.

Garnet, omphacite, platy amphibole, quartz and rutile are interpreted as the peak metamorphic assemblage based upon their granular texture; the presence of quartz, omphacite and rutile throughout garnet grains; and platy amphibole sharing straight grain boundaries with garnet and omphacite. Symplectitic

amphibole, plagioclase, titanite, ilmenite, epidote, K-feldspar, biotite and muscovite are all interpreted to have grown during retrograde metamorphism of the peak phases due to their association with retrograde microstructures (e.g., coronae) and their anhedral morphologies.

### 3.3 | Felsic Gneiss (GE17)

Sample GE17 was acquired from the felsic portion of a layered mafic and felsic outcrop (Figure 5a). We sampled the felsic domain as the mafic domain is similar to sample GE3, and study of this sample enables a comparison of how eclogite-facies metamorphism is recorded in differing bulk compositions.

Sample GE17 consists of plagioclase (61 vol.%), clinozoisite (14 vol.%), garnet (8 vol.%), muscovite (6 vol.%), omphacite (4 vol.%), quartz (3 vol.%) and kyanite (2 vol.%) plus accessory titanite, amphibole, apatite, rutile, chlorite, biotite, magnetite, iron sulphides, ilmenite and zircon (Figure 5b). The sample features a gneissic texture, resulting from compositional banding and the alignment of clinozoisite grains.

Plagioclase is mainly 100−200 μm across and exhibits an anhedral to faceted aspect. Plagioclase is compositionally oligoclase ($X_{Ab}$ = 0.70−0.82), with grain cores displaying the highest albite content. Straight grain boundaries with omphacite and garnet
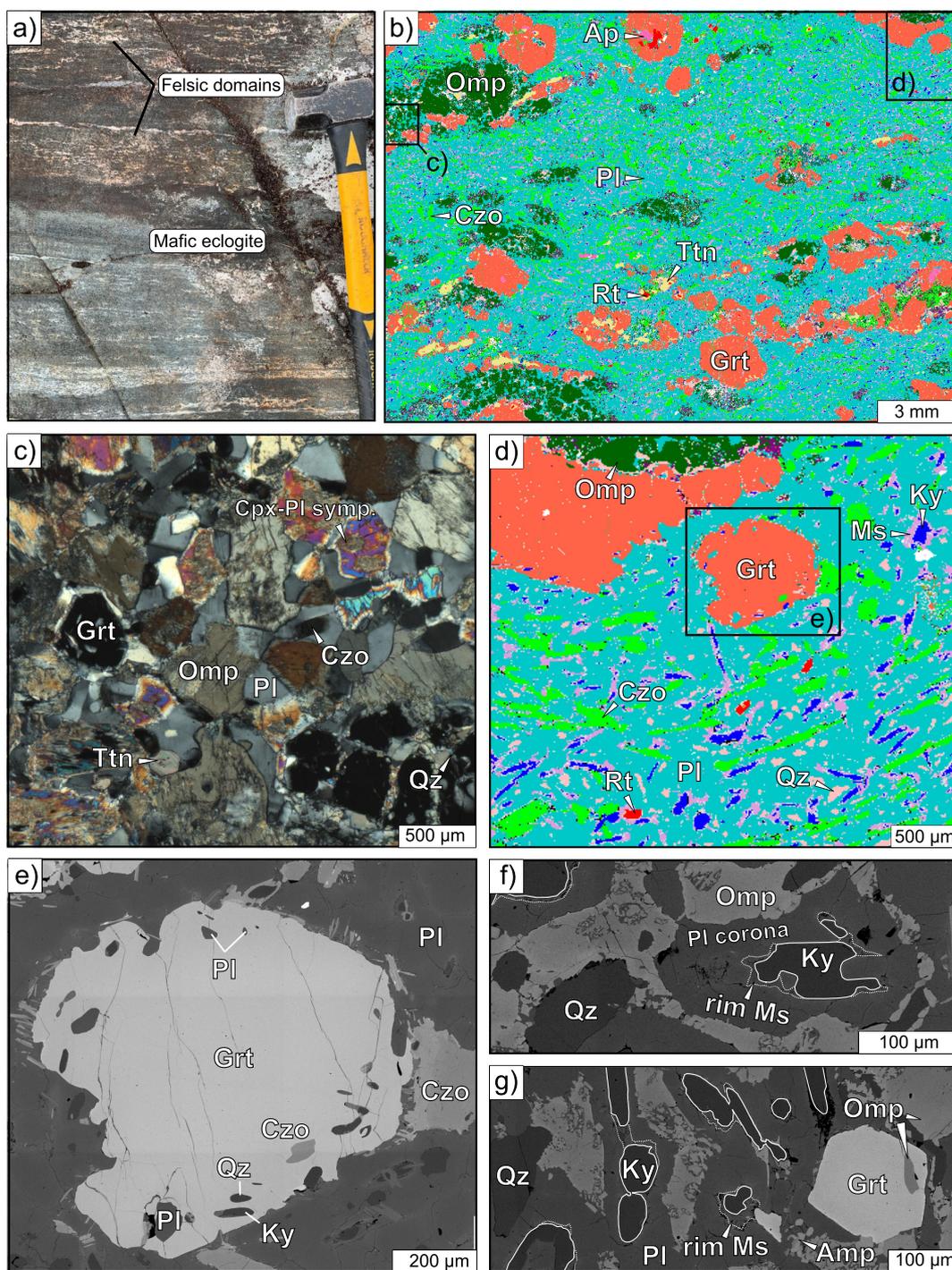
**FIGURE 5** | Felsic gneiss sample GE17 petrography. (a) Photograph of the layered outcrop from which sample GE17 was collected. (b) QEMSCAN phase map showing a gneissic fabric defined by weak compositional banding. (c) Photomicrograph viewed under crossed polars of the boxed area in (b) showing a mosaic of omphacite, plagioclase and garnet grains. (d) Enlarged QEMSCAN phase map of an area demarcated in (b) showing clinozoisite grains aligned with the gneissic fabric, and muscovite present as both a matrix phase and embaying kyanite grains. (e) Back-scattered electron (BSE) image of the area highlighted in (d), showing a subhedral garnet porphyroblast with an inclusion-rich rim containing kyanite, clinozoisite, plagioclase and quartz. (f) BSE image showing a resorbed kyanite grain surrounded by a muscovite and plagioclase corona. (g) BSE image showing a euhedral garnet porphyroblast.

are common (Figure 5c) and are interpreted to indicate an equilibrium relationship among these phases. Clinozoisite occurs as anhedral to euhedral laths that are chemically zoned, with the pistacite content $\left(\frac{Fe^{3+}}{Fe^{3+} + Al}\right)$ increasing from 0.01 to 0.10 from core to rim (Figure 5d).

Garnet forms anhedral to euhedral grains up to ~3 mm in diameter (Figure 5b–e,g). Garnet chemistry features a compositionally flat inner core ($Alm_{49}Prp_{32}Grs_{18}Sps_1$) and a more grossular-rich inner rim plateau ($Alm_{39}Prp_{24}Grs_{37}Sps_1$) (Figure 4). Inclusions are common and primarily consist of kyanite, plagioclase,

quartz, omphacite, titanite, apatite, rutile with minor K-feldspar and clinozoisite (Figure 5b,d,e,g). Muscovite (3.00–3.12 Si pfu) occurs mainly as overgrowths of anhedral kyanite (Figure 5f,g) and as <50 μm of matrix laths.

Omphacite is up to ~1 mm across and occurs as anhedral to euhedral grains. Individual grains are compositionally homogeneous, but compositions vary between grains from $Di_{61}Jd_{26}Hed_{13}Aeg_8$ to $Di_{42}Jd_{44}Hed_{14}Aeg_0$ (~0.30–0.50 Al pfu), with the former being more dominant (Figure 4). Omphacite inclusions primarily consist of plagioclase, titanite, quartz and rutile. Quartz occurs as anhedral grains in the matrix. Kyanite is mainly anhedral and is almost always separated from omphacite by a plagioclase rim (Figure 5f,g). Rutile grains are up to ~0.5 mm across, contain ilmenite lamellae and occur as inclusions and matrix grains. Titanite is present as anhedral matrix clusters, sometimes rimming rutile, and as inclusions (Figure 5b). K-feldspar mostly occurs as clustered anhedral matrix grains co-occurring with biotite, with both phases replacing muscovite. Amphibole and chlorite are volumetrically minor phases and are concentrated along fractures.

Plagioclase, garnet, omphacite, quartz, kyanite, clinozoisite, rutile and muscovite are interpreted as the peak metamorphic assemblage based upon: The occurrence of all of these phases, bar muscovite, as inclusions in garnet rims (Figure 5e) and their shared straight grains boundaries in the matrix. Kyanite is the exception to the latter point as it is surrounded by muscovite-plagioclase rims, which are a typical retrograde microstructure, implying that some plagioclase and muscovite are also retrograde (Figure 5f,g). K-feldspar and titanite were present during prograde metamorphism as they form facetted inclusions in garnet and omphacite, but they are only present as retrograde phases in the matrix. Minor amphibole and ilmenite are interpreted to have grown during retrograde metamorphism of the peak phases due to their anhedral habit and association with grain boundaries and fractures.

## 4 | U-Pb Geochronology

Zircon and rutile hosted within mafic eclogite sample GE3 and felsic gneiss sample GE17 were targeted for in situ U-Pb geochronology, to constrain the timing of metamorphism and retrogression.

### 4.1 | Methods

Back-scattered electron (BSE) and secondary electron (SE) images were acquired for zircon and rutile to characterise grain morphologies, zoning, locations, cracks and inclusion suites. Cathodoluminscence (CL) images were additionally acquired for zircon to aid with data collection and interpretation (e.g., Figure 6a–h). All images were acquired using a FEI Quanta 650 FEG Scanning Electron Microscope at the University of Cambridge.

In situ U-Pb zircon and rutile analyses were performed by laser ablation inductively coupled plasma mass spectrometry (LA-ICP-MS) at the University of Portsmouth, UK, using an ASI RESOlution 193 nm ArF excimer laser coupled to an Agilent 8900 triple quadrupole ICP-MS. Data are provided in Tables S2–S4, and full analytical methods are in Table S5. Age

calculations were performed using the programme IsoplotR (Vermeesch 2018).

Analyses of zircon were performed during two sessions, initially for U-Pb only using a 14 μm spot and then for coupled U-Pb and trace elements, using a 38 μm spot. Repetition rate was 2 Hz, and fluence was ~2.5 J/cm². For U-Pb analyses, zircon 'BB9' was used as the primary standard (Santos et al. 2017), and zircons 'Plesovice' (Sláma et al. 2008), 'GJ-1' (Jackson et al. 2004) and '91500' (Wiedenbeck et al. 1995) were used as secondary standards. For trace element analyses, glass 'NIST 614' was used as a primary standard (Jochum et al. 2011), and glass 'NIST 612' (Jochum et al. 2011), glass 'BCR-2G (Jochum et al. 2005) and zircon '91500' (Wiedenbeck et al. 1995) were used as secondary standards. Overall reproducibility achieved on the secondary standards was <2% for U-Pb ages and <15% for trace elements. Following the recommendations of Spencer, Kirkland, and Taylor (2016), we report single age estimates using the $^{206}Pb/^{238}U$ system if younger than ~1.5 Ga and $^{207}Pb/^{206}Pb$ if older. We report populations using concordia ages (Ludwig 1998), with mean square weighted deviation (MSWD) of concordance plus equivalence given as a measure of goodness-of-fit (Ludwig 1998; Vermeesch 2018). Reported uncertainties are ± 2σ propagated by quadrature for uncertainty on the primary standard with an additional 2% for long-term reproducibility. Concordia age uncertainties are additionally augmented by a factor of $\sqrt{MSWD}$ for overdispersion (Vermeesch 2018).

In situ U-Pb rutile analyses were carried out in parallel with zircon analyses as described above. Isotopic U-Pb analyses were acquired during three sessions using two spot sizes (80 and 50 μm spots), depending on the grain size of the rutile. Repetition rate was 5 Hz, and fluence was ~3.5 J/cm². For U-Pb analyses, rutile 'R10' was used as a primary standard (Luvizotto and Zack 2009), and rutiles 'R13' (Schmitt and Zack 2012) and 'R19' (Zack et al. 2011) were used as secondary standards. For trace element analyses, glass 'NIST 610' was used as a primary standard (Jochum et al. 2011), and glass 'BHVO-2G' (Jochum et al. 2005) and rutile 'R10' (Luvizotto and Zack 2009) were used as secondary standards. Overall reproducibility achieved on the secondary standards was <1% for U-Pb ages and <13% for trace elements. Data filtering procedures for trace elements are described in the Supporting Information section. We analyse U-Pb rutile data using Tera–Wasserburg plots. Uncertainties are calculated as done for U-Pb zircon concordia ages.

### 4.2 | Zircon Characterisation

Zircon in mafic eclogite GE3 occurs as anhedral to euhedral grains 5–50 μm in diameter, mostly within the matrix. Inclusions are common and consist of garnet, omphacite and quartz (Figure 6a,b). CL imaging reveals grains mainly exhibit patchy zoning, with irregular concentric zoning and diffuse zoning being less common (Figure S2). Zircon in felsic gneiss GE17 occurs as anhedral to subhedral grains 20–100 μm in diameter (Figure 6c,g), occurring equally as inclusions and within the matrix. Inclusions are not observed within these zircon grains. CL images generally show diffuse zoning (Figure 6d–f) and in some cases distinct core and rim domains, with the rim domains commonly exhibiting more diffuse zoning (Figure 6h).
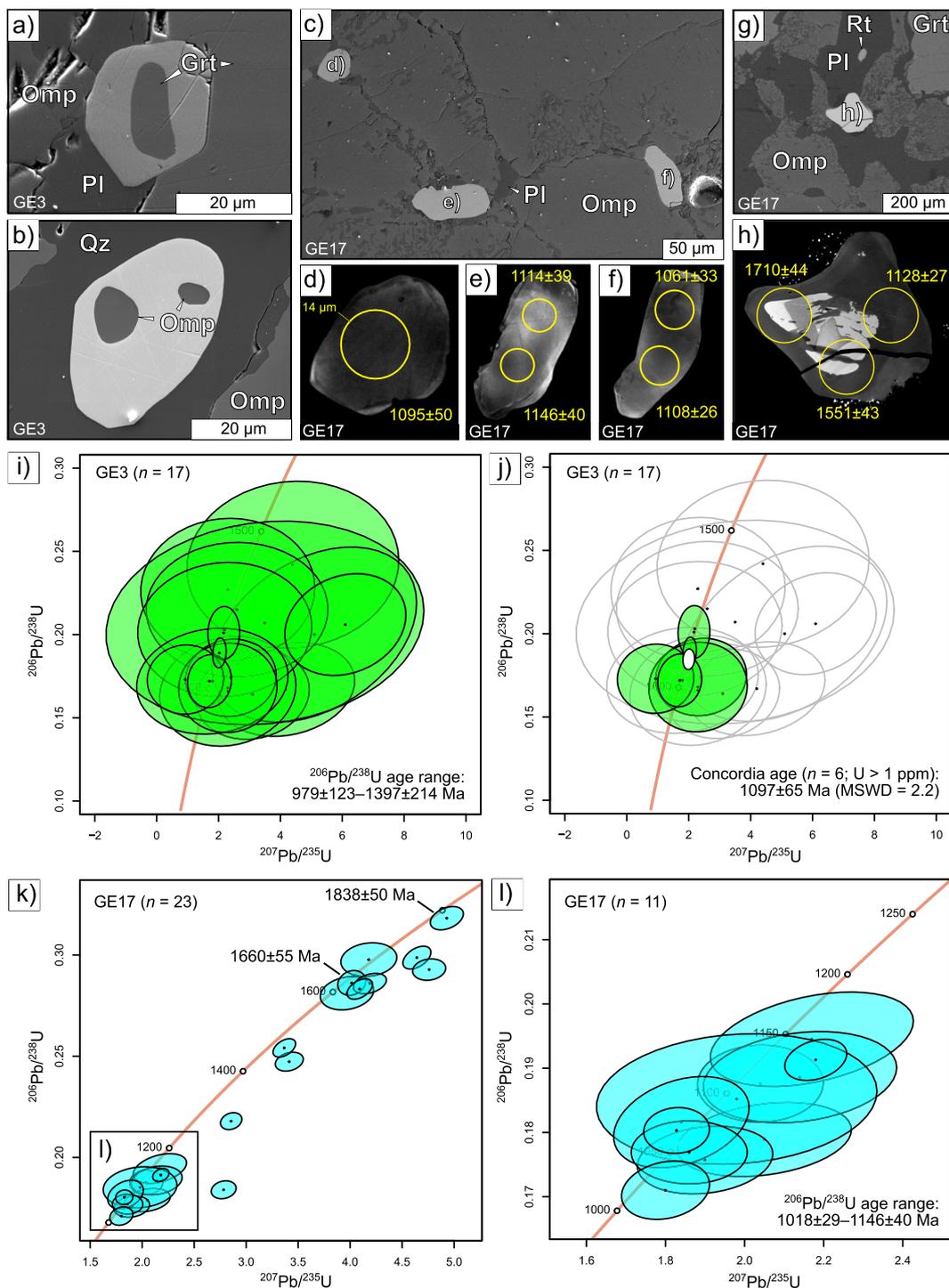
**FIGURE 6** | Secondary electron (SE), back-scattered electron (BSE) and cathodoluminescence (CL) images of zircon grains from samples GE3 (a,b) and GE17 (c–h), and the results of U-Pb zircon dating. Yellow circles denote ~14 μm of ablation spots. (a,b) SE images of zircons hosting inclusions of garnet and omphacite. (c) SE image of matrix zircon grains. (d–f) CL images showing diffuse zoning in the zircon grains displayed in (c). (g) BSE image of a matrix zircon. (h) CL image of the zircon in (g) showing distinct core and rim domains. (i) Concordia plot of the full sample GE3 dataset (n = 17). (j) Subset of analyses with U > 1 ppm (n = 6) from (i). (k) Concordia plot of the full sample GE17 dataset (n = 23). (l) Subset of analyses in boxed region of (k) (n = 11).

## 4.3 | U-Pb Zircon Results

From mafic eclogite sample GE3, a total of 43 U-Pb zircon analyses were obtained. These analyses yielded relatively imprecise ages due to the low U and radiogenic Pb content of the analysed grains (typically <1 and <0.1 ppm, respectively). Due to

the small sizes of the analysed zircon grains (<50 μm), only 17 analyses resided solely within the grains (Figure 6i). This reduced dataset gives a concordia age of $1102 \pm 72$ Ma (MSWD = 3.0, n = 17), but the MSWD value indicates that these data do not define a single population (Spencer, Kirkland, and Taylor 2016). No petrographic or textural criteria could be

applied to further refine this population, which ranges from $979 \pm 123$ Ma to $1397 \pm 214$ Ma (Figure 6i). However, if we only consider grains with U > 1 ppm, then these data yield a concordia age of $1097 \pm 65$ Ma ($n = 6$; Figure 6j), with an acceptable MSWD value of 2.2 (Spencer, Kirkland, and Taylor 2016). Based on the occurrence of garnet and clinopyroxene as inclusions in zircon (Figure 6a,b), this age is interpreted to record high-pressure metamorphism.

From felsic gneiss sample GE17, a total of 28 zircon analyses were obtained, of which 23 remain after discarding spots that hit matrix phases. This dataset is higher precision than obtained from sample GE3 as the zircons contain higher U (>8 ppm) and radiogenic Pb (>0.2 ppm). The dataset features a cluster in the interval $1018 \pm 28$ to $1146 \pm 40$ Ma, and dispersed analyses form a discordia line back to $1838 \pm 50$ Ma (Figure 6k). The older analyses were acquired from grains that typically feature bright cores in CL, but all analyses partially include rim regions (e.g., Figure 6h) such that an age cannot be resolved. Nevertheless, the oldest single age of $1838 \pm 50$ Ma is consistent with previously documented Paleoproterozoic protolith ages for these units (Brewer et al. 2003; Bird et al. 2023).

The younger cluster features 11 analyses of five zircon grains, all in the matrix, mostly displaying diffuse CL zoning (Figure 6d–f). Two of these analyses do not touch concordia within their uncertainties. Excluding these two analyses, the population yields a concordia age of $1069 \pm 46$ Ma (MSWD = 5.3, $n = 9$), but the MSWD indicates that these data do not define a single population (Spencer, Kirkland, and Taylor 2016). No petrographic or textural criteria could be applied to further refine this population, so we report the range $1018 \pm 29$ to $1146 \pm 40$ Ma. Based on the weak and diffuse zoning, rounded morphology and association with rim zones (where present, e.g., Figure 6h), this age range is interpreted to represent metamorphic growth (Zheng et al. 2022). The metamorphic age for sample GE3, tied to high pressure metamorphism based on the inclusion suite, overlaps with the range for GE17.

## 4.4 | Rutile Characterisation

Rutile occurs as anhedral to euhedral grains up to ~350 µm in diameter, as both inclusions hosted in garnet, omphacite, quartz and amphibole and within the matrix (Figure 7a,b).
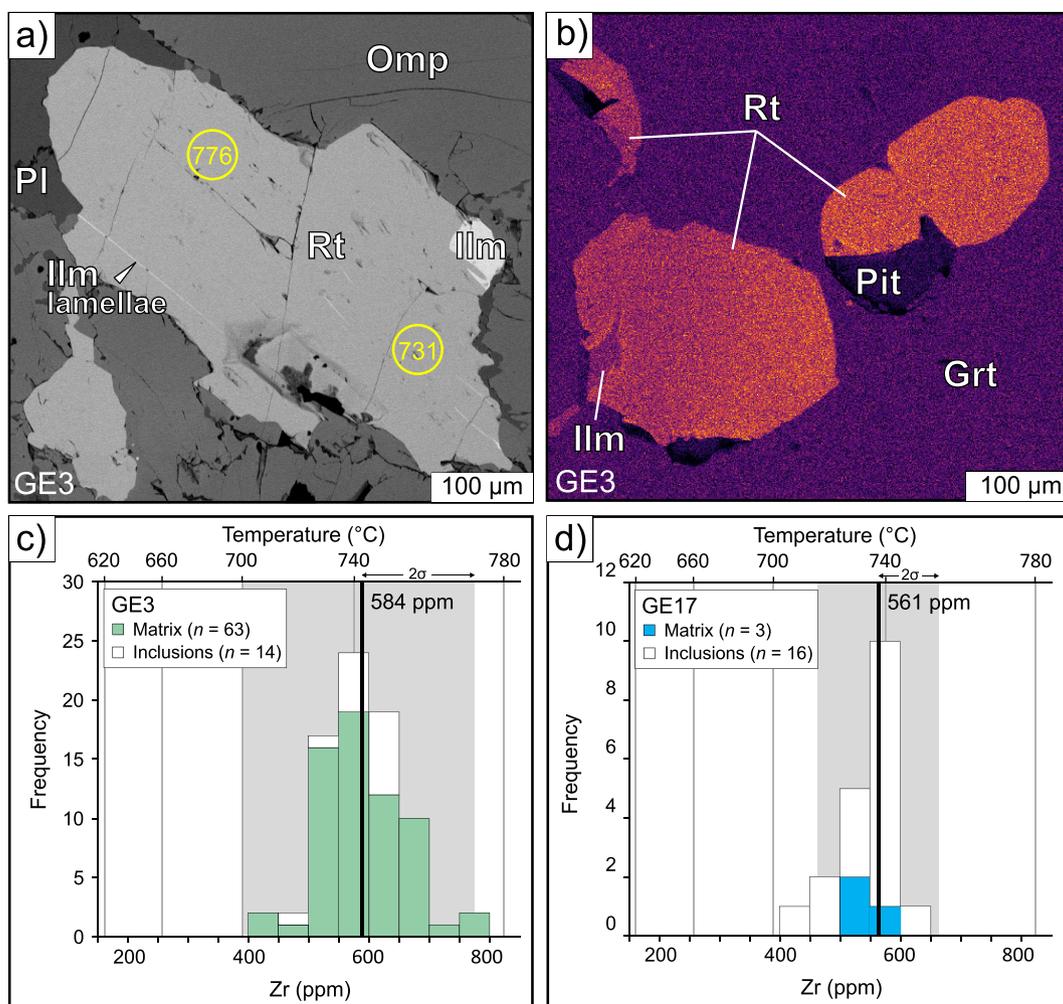


**FIGURE 7** | Zr-in-rutile thermometry results. (a) Back-scattered electron image of a rutile grain, overlain by yellow circles showing analytical spot locations and resultant temperatures. Ablation spots are 50 µm. (b) X-ray intensity map of Zr in inclusion rutile grains, showing asymmetric and homogeneous zoning patterns. (c) Stacked histogram of the filtered Zr-in-rutile dataset for sample GE3, colour coded by petrographic location. Temperatures corresponding to the measured concentrations are also shown, assuming $P = 20$ kbar; see text for discussion. (d) As (c) but for sample GE17. Median Zr-in-rutile temperatures with associated $2\sigma$ uncertainties are shown.

Matrix grains exhibit a range of morphologies, including as grains with faceted or corroded margins and as multi-faceted aggregates, while inclusion grains are commonly faceted. Rutile grains are inclusion-free but commonly show ilmenite lamellae and partial replacement by ilmenite at rutile grain margins.

## 4.5 | U-Pb Rutile Results

A total of 166 rutile analyses were obtained from sample GE3, and 29 from sample GE17. After discarding spots that hit matrix phases, 119 analyses remain from GE3 and 21 from GE17. The GE3 dataset yields a $^{206}Pb/^{238}U$ intercept age of $424 \pm 9$ Ma (MSWD = 1.6, $n$ = 119; Figure S3). An overlapping $^{206}Pb/^{238}U$ intercept age of $413 \pm 17$ Ma (MSWD = 1.4, $n$ = 21; Figure S4) was obtained from the GE17 dataset. These rutile ages record Caledonian metamorphism based on the ages corresponding to the time of peak metamorphism attained during the terminal ('Scandian') phase of the Caledonian event (437–415 Ma; Searle 2022), which in the Glenelg inlier is represented by lower amphibolite-facies assemblages (Storey 2002; Storey, Brewer, and Parrish 2004). Such ages are consistent with previous age determinations from the Eastern Unit (Brewer et al. 2003; Bird et al. 2023) and surrounding Moine nappe rocks (Searle 2022). Petrographically, the rutile grains are interpreted to belong to the eclogite-facies mineral assemblage. The U-Pb rutile system was therefore reset during Caledonian metamorphism.

## 4.6 | Interpretation of Age Data

The results of U-Pb zircon and rutile dating are presented in Figure 8, along with published metamorphic ages from the Eastern Unit of the Glenelg inlier and maximum deposition ages from the Neoproterozoic successions of focus in this study. Our U-Pb zircon estimates of $1097 \pm 65$ Ma (sample GE3) and $1146 \pm 40$ Ma to $1018 \pm 28$ Ma (sample GE17) fall within the predicted interval for peak eclogite-facies metamorphism when considering previous constraints for the timing of burial (c. 1.2–1.1 Ga; Bird et al. 2023) and partial exhumation (c. 1.0–0.9 Ga; Sanders, van Calsteren, and Hawkesworth 1984; Brewer et al. 2003; Bird et al. 2023). This overall timeframe overlaps with deposition of the Neoproterozoic successions in northwest Scotland, which surround the Glenelg inlier and the Grenville and Sveconorwegian orogenies (Figure 8; Rivers 1997; Rivers et al. 2012; Bingen et al. 2021). We discuss the sedimentary successions and their importance for constraining the eclogites' provenance below.

## 5 | Zr-in-Rutile and Ti-in-Zircon Thermometry

## 5.1 | Methods

In situ trace element rutile and zircon analyses were performed by ICP-MS following the same methods as described above for U-Pb zircon and rutile geochronology. Trace elements were acquired using a 38 μm spot for zircon and an 80 μm spot for rutile. Trace element data are provided in Table S2
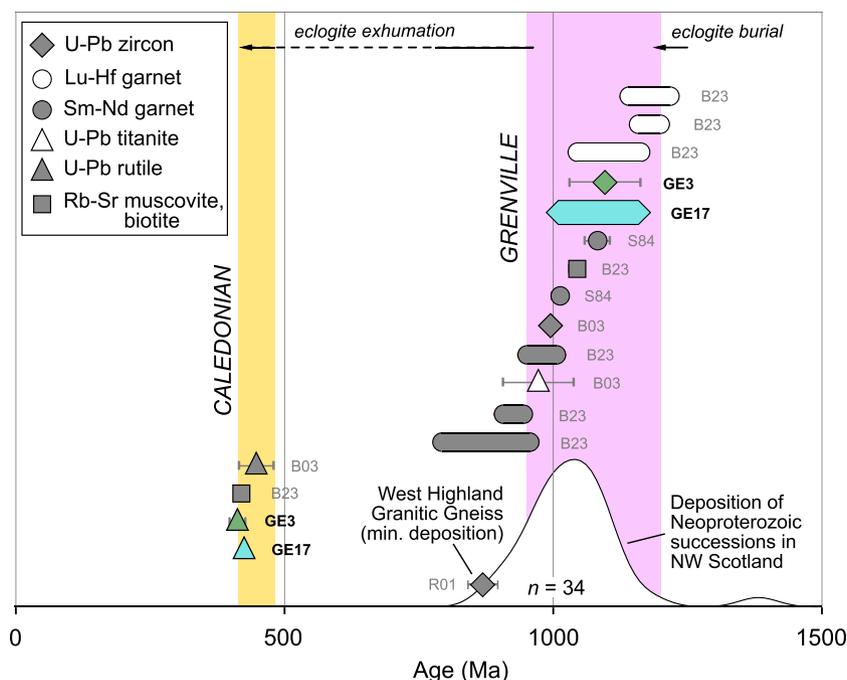


**FIGURE 8** | U-Pb zircon and rutile results from this study (samples GE3 and GE17) plotted alongside published metamorphic age data from the Eastern Unit of the Glenelg inlier. S84 = Sanders, van Calsteren, and Hawkesworth 1984; B03 = Brewer et al. 2003; B23 = Bird et al. 2023. Dashed arrows denote the approximate timing of eclogite burial and exhumation based on the published age data. Maximum deposition age data ($n$ = 34) from the Sleat and Torridon Groups (Caledonian foreland), Morar Group (Moine nappe) and Glenfinnan and Loch Eil Groups (Sgurr Beag nappe) are shown in a kernel density plot. These data are a combination of U-Pb zircon estimates (only youngest detrital ages and age peaks; Rainbird, Hamilton, and Young 2001; Rogers et al. 2001; Peters 2001; Friend et al. 2003; Cawood et al. 2004; Cawood et al. 2015; Kirkland, Strachan, and Prave 2008; Krabbendam et al. 2017) and a Rb-Sr whole-rock estimate for diagenesis (Turnbull, Whitehouse, and Moorbath 1996).

(zircon) and Table S3 (rutile), and full analytical methods are in Table S5. Data reduction procedures are described in the Supporting Information section. Qualitative X-ray maps were generated for a subset of rutile grains using a JEOL JXA-iHP200F Field Emission electron probe micro-analyser at the University of Cambridge, operating at 20 kV with a focused 1 μm spot. Beam current was 200 nA, and dwell time was 500 ms, with Zr ($L\alpha$) on the PETL crystal.

Zr-in-rutile temperatures were calculated using the 'combined dataset' calibration of Kohn (2020), with a two-sigma uncertainty of $\pm10°C–15°C$. The samples are suitable for this thermometer as they contain abundant quartz and zircon such that $SiO_2$ and $ZrO_2$ are well buffered (Kohn 2020). Ti-in-zircon temperatures were calculated using the calibration of Crisp et al. (2023). The samples are suitable for this thermometer as they contain abundant rutile and quartz such that $aTiO_2 = 1$ and $aSiO_2 = 1$ (Crisp et al. 2023). Reported temperatures below assume an input pressure of 20 kbar according to the estimates of Rawson, Carswell, and Smallwood (2001) and Storey, Brewer, and Temperley (2005) for the Glenelg eclogites. However, for reasons discussed below, our final quoted temperatures for the eclogites are obtained using the range of pressures bounding assemblage fields from $P–T$ pseudosections for samples GE3 and GE17.

## 5.2 | Zr-in-Rutile Results

From sample GE3, a total of 99 trace element analyses were obtained from rutile, of which 77 remain following data reduction (see Supporting Information). Zirconium values range from 420 to 797 ppm (707°C–776°C) and are concentrated around a median of $584 \pm 131$ ppm ($742^{+22o}_{-27}$C), with the distribution uncertainty quoted at $2\sigma$ (Figure 7c). Matrix and inclusion rutile grains have a similar Zr distribution. Zirconium varies by up to ~300 ppm (~45°C) within the largest grains where multiple spots were possible (Figure 7a).

From sample GE17, a total of 20 trace element analyses were obtained, of which 19 remain following data reduction. Zr values range from 420 to 619 ppm (707°C–748°C) and are concentrated around a median of $561 \pm 100$ ppm ($737^{+18o}_{-21}$C; Figure 7d). Only three grains occur in the matrix, with their Zr values centred around the dataset median. Multispot analyses from four rutile grains indicate grain-scale variation in Zr of up to ~128 ppm (~28°C). Intragrain variation with respect to Zr in samples GE3 and GE17 is mainly from asymmetric zoning, as revealed by qualitative X-ray maps of matrix and inclusion grains (e.g., Figure 7b).

## 5.3 | Ti-in-Zircon Results

A total of 16 trace element and isotopic U-Pb analyses were obtained from zircon grains in sample GE17. One analysis yields a concordant $^{206}Pb/^{238}U$ age of $1069 \pm 27$ Ma, with a corresponding Ti-in-zircon value and temperature of 15.16 ppm and 823°C. Two additional analyses yield consistent $^{206}Pb/^{238}U$ ages within the quoted uncertainties, but they do not touch concordia: $1089 \pm 29$ Ma and 6.49 ppm (738°C) and $1128 \pm 27$ Ma and 6.64 ppm (740°C). The minimum $2\sigma$ calibration uncertainty on these temperature estimates is 65°C (Crisp et al.

2023). Calculated Eu anomalies ($Eu/Eu* = Eu_N/[Sm_N \times Gd_N]^{0.5}$, with 'N' denoting values normalised to chondrite after McDonough and Sun 1995) from these zircons are relatively small, in the range 0.74–0.89, consistent with zircon growth in a feldspar-poor eclogite-facies rock (i.e., at the upper end of 16–19 kbar pressure range for this sample, where plagioclase is volumetrically minor as a peak phase; Figure 10b).

## 5.4 | Interpretation of $T$ Data

The Zr-in-rutile datasets from samples GE3 and GE17 yield consistent median temperatures of $742^{+22}_{-27}$°C (GE3) and $737^{+18o}_{-21}$°C (GE17), recorded in both matrix and inclusion grains (Figure 7c,d). The observed asymmetric zoning is consistent with minimal Zr loss via diffusion given that a radial zoning pattern characteristic of diffusion is not observed (Cherniak, Manchester, and Watson 2007). The Ti-in-zircon dataset from sample GE17 is limited to three grains with Grenville ages, yielding temperatures of 738°C to 823°C. As there are few data, and the range is encompassed by the Zr-in-rutile dataset, we do not use Ti-in-zircon thermometry for final $P–T$ determination.

Despite the Caledonian age obtained from the U-Pb rutile analyses, the Zr-in-rutile temperatures are interpreted to record Grenville-aged eclogite-facies metamorphism. This view is supported by the following evidence: (1) rutile is interpreted as a peak eclogite-facies phase; (2) the constrained Zr-in-rutile temperatures exceed conditions for Caledonian metamorphism across the Moine nappe (420°C–680°C; Thigpen et al. 2013; Ashley, Thigpen, and Law 2015; Mazza et al. 2018); (3) the preservation of asymmetric zoning of Zr in rutile grains (e.g., Figure 7b), implying relatively little or no modification; and (4) consistency between the Ti-in-zircon and Zr-in-rutile temperature estimates. Decoupling of Zr from the U-Pb system, as implied here, has been previously reported in metamorphic rocks (Kooijman et al. 2012; Zhang et al. 2014; Ewing et al. 2015) and is attributed to the lower diffusivity of Zr in rutile compared to Pb, by up to one order of magnitude (Cherniak, Manchester, and Watson 2007). We quote the temperature ranges encompassed by $2\sigma$ uncertainties surrounding the distribution medians as best representing the conditions of eclogite-facies metamorphism: 715°C–764°C for GE3 and 716°C–755°C for GE17 (at 20 kbar).

## 6 | Phase Equilibrium Modelling

### 6.1 | Methods

Phase equilibrium modelling was performed on samples GE3 and GE17 using Theriak-Domino (version 11-Mar-2020 de Capitani and Petrakakis 2010), with the thermodynamic dataset ds62 (Holland and Powell 2011). The model system $Na_2O-CaO-K_2O-FeO-MgO-Al_2O_3-SiO_2-H_2O-TiO_2-O$ (NCKFMASHTO) was used for mafic sample GE3, with MnO additionally considered for felsic sample GE17, using the following activity-composition models: garnet, orthopyroxene, biotite and ilmenite (White et al. 2014); omphacitic clinopyroxene and melt (Green et al. 2016); clino-amphibole (Green et al. 2016); plagioclase–K-feldspar (Holland, Green, and

Powell 2022); epidote (Holland and Powell 2011); and muscovite (Coggon and Holland 2002; White et al. 2014). Pure phases included albite, coesite, $H_2O$, lawsonite, quartz, rutile, titanite and zoisite.

Model bulk rock compositions were calculated using measured mineral modes in combination with representative mineral compositions (Table S1). Phases outside the model system were ignored and measured modes renormalised. Garnet and omphacite were idealised to conform to the stoichiometric criteria of their $a$–$X$ models; for example, tetrahedral Si in garnet was set as 3 cpfu. For mafic sample GE3, only the compositionally homogeneous outer shell of garnet was considered as part of the effective bulk composition (equivalent to 69% of its volume; Figure 4). Bulk compositions are listed in Table 1. Stoichiometric estimates of $H_2O$ contents were 0.42 mol% for mafic sample GE3 and 2.23 mol% for felsic sample GE17.

## 6.2 | P–T Results

*Mafic eclogite GE3.* Figure 9a shows a *P–T* pseudosection for mafic sample GE3. The interpreted peak assemblage (garnet,

omphacite, rutile, amphibole and quartz) is not present as a unique field on the pseudosection but dominates the assemblages at pressures below the upper limit of amphibole stability (purple line). The presence of biotite (brown line) to lower pressures, which was interpreted as a retrograde phase, and the stability of a second clinopyroxene phase (green line) to lower temperatures, which was not observed, delimit a triangular region that exhibits the best match to petrographic observations. These fields are highlighted by red text and feature the additional phases of muscovite, liquid and/or vapour. All three phases are present in minor proportions (<1 vol.%) and could viably have been present at peak conditions with the record of these phases now obscured by retrogression.

The triangular region overlaps with the Zr-in-rutile temperature constraints outlined above, in the region 18–20.3 kbar and 706°C–760°C (red polygon, Figure 9b). At 750°C, the modelled phase mode of clinopyroxene exhibits a good match to QEMSCAN measurements in this pressure range (red line, Figure 9c). The modelled garnet mode is slightly higher than the measured value above 18 kbar, consistent with the partial replacement of garnet rims by amphibole and/or plagioclase. Conversely, the modelled amphibole mode is lower than

**TABLE 1** | Sample GE3 and GE17 bulk compositions used for phase equilibrium modelling (mol.).

| Sample | Si | Al | Ca | Mg | Fe | K | Na | Ti | Mn | H | O | $X_{Fe^{3+}}$ | $X_{Mg}$ |
|---|---|---|---|---|---|---|---|---|---|---|---|---|---|
| GE3 | 52.69 | 15.21 | 12.73 | 12.52 | 10.13 | 0.15 | 4.55 | 1.06 | 0 | 0.83 | 168.96 | 0.07 | 0.57 |
| GE17 | 60.10 | 32.15 | 10.58 | 1.92 | 2.40 | 1.23 | 11.05 | 0.37 | 0.03 | 4.46 | 192.62 | 0.13 | 0.44 |

*Note:* $X_{Fe^{3+}} = Fe^{3+}/(Fe^{2+} + Fe^{3+})$; $X_{Mg} = Mg/(Mg + Fe^{2+})$.
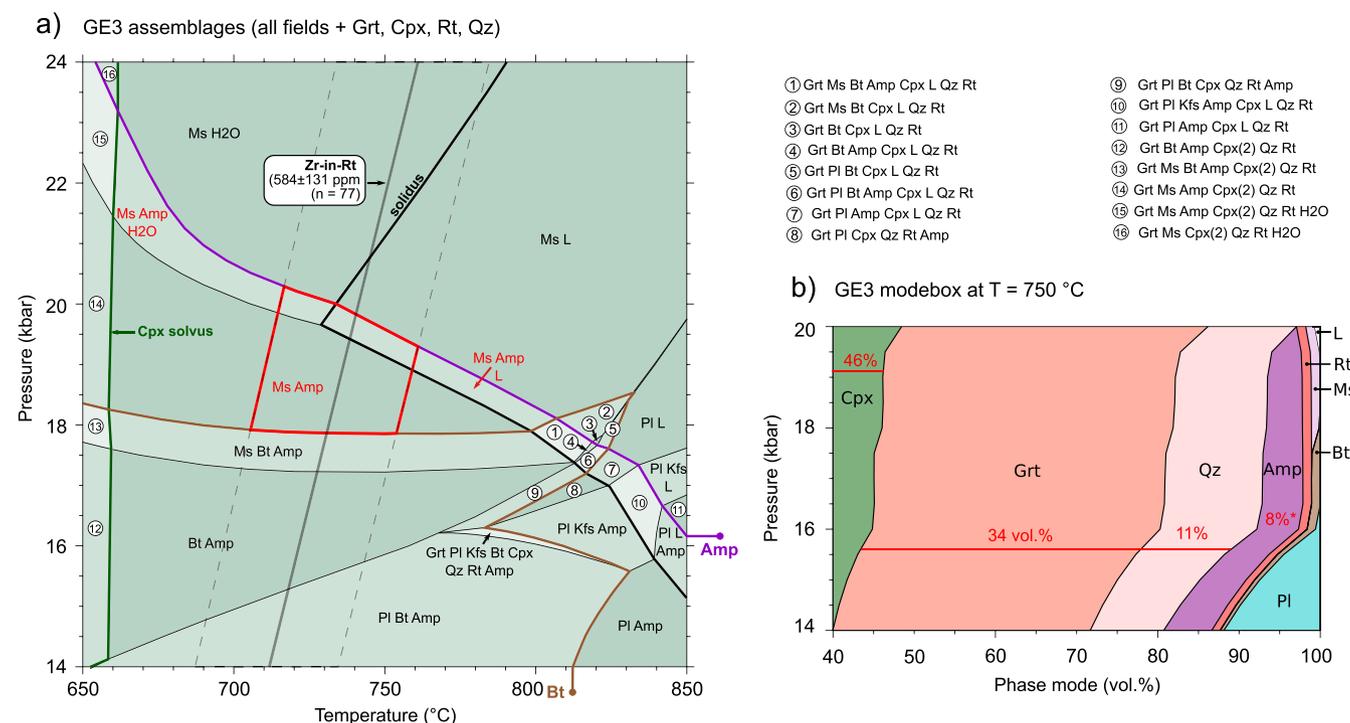


**FIGURE 9** | Sample GE3 pseudosection modelling. (a) *P–T* pseudosection with the viable peak assemblages shown in red text; see text for discussion. The median Zr-in-rutile temperature range is shown with a two-sigma envelope (dashed grey lines). The best estimate of peak conditions is demarcated by the red polygon. (b) Modebox plot at 750°C with QEMSCAN-derived phase modes shown by red lines. The measured amphibole mode (8%*) occurs outside the plot's lower bound (i.e., <14 kbar).
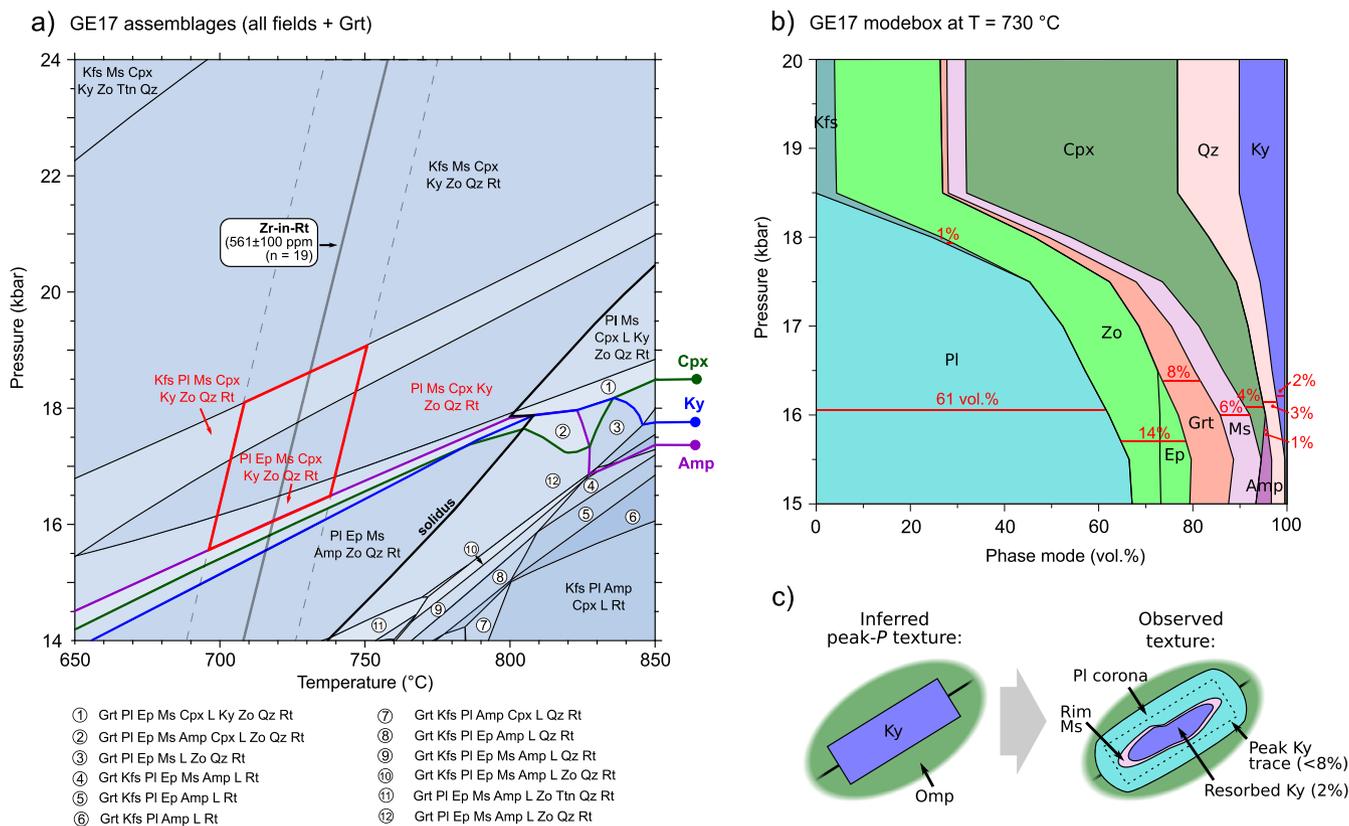
13 of 26

**a)** GE17 assemblages (all fields + Grt)

**b)** GE17 modebox at T = 730 °C

① Grt Pl Ep Ms Cpx L Ky Zo Qz Rt
② Grt Pl Ep Ms Amp Cpx L Zo Qz Rt
③ Grt Pl Ep Ms L Zo Qz Rt
④ Grt Kfs Pl Ep Ms Amp L Rt
⑤ Grt Kfs Pl Ep Amp L Rt
⑥ Grt Kfs Pl Amp L Rt
⑦ Grt Kfs Pl Amp Cpx L Qz Rt
⑧ Grt Kfs Pl Ep Amp L Qz Rt
⑨ Grt Kfs Pl Ep Ms Amp L Qz Rt
⑩ Grt Kfs Pl Ep Ms Amp L Zo Qz Rt
⑪ Grt Pl Ep Ms Amp L Zo Ttn Qz Rt
⑫ Grt Pl Ep Ms Amp L Zo Qz Rt

**c)** Inferred peak-P texture: → Observed texture:

**FIGURE 10** | Sample GE17 pseudosection modelling. (a) *P–T* pseudosection with the viable peak assemblages shown in red text. The median Zr-in-rutile temperature range is shown with a two-sigma envelope (dashed grey lines). The best estimate of peak conditions is demarcated by the red polygon. (b) Modebox plot at 730°C with QEMSCAN-derived phase modes shown by red lines. (c) Sketches show the interpreted development of clinopyroxene-kyanite-plagioclase-muscovite microstructures.

measured in this 18–20 kbar range, consistent with the observations of additional retrograde amphibole in the sample.

*Felsic gneiss GE17.* Figure 10a shows a *P–T* pseudosection for the felsic gneiss sample GE17. The interpreted peak assemblage (plagioclase, garnet, omphacite, quartz, kyanite, clinozoisite and rutile and muscovite) is present in a triangular field that covers a large *P–T* range from 15.5 to 21 kbar and 650°C to >850°C. To higher temperatures, the fluid-undersaturated solidus is encountered. To higher and lower pressures, K-feldspar and epidote join the assemblage, respectively. Neither pressure boundary is considered a strong constraint, owing to K-feldspar being present as inclusions in garnet, and epidote-zoisite stability being strongly controlled by the imposed $Fe^{3+}$ content, which is poorly constrained. Therefore, these fields are also considered viable, and highlighted by red text. To slightly higher and lower pressures, plagioclase is lost and amphibole is stabilised, respectively. Both of these boundaries impose strong constraints on viable pressures, given the high proportion of observed plagioclase, and the unambiguous interpretation of amphibole as a retrograde phase in this sample.

The Zr-in-rutile results are used to delimit the potential peak fields further, indicating peak conditions of 15.5–19 kbar and 695°C–750°C (red polygon, Figure 10a). A modebox constructed for sample GE17 at 730°C (Figure 10b) across pressures that bound the peak fields shows that this region of *P–T* space features significant
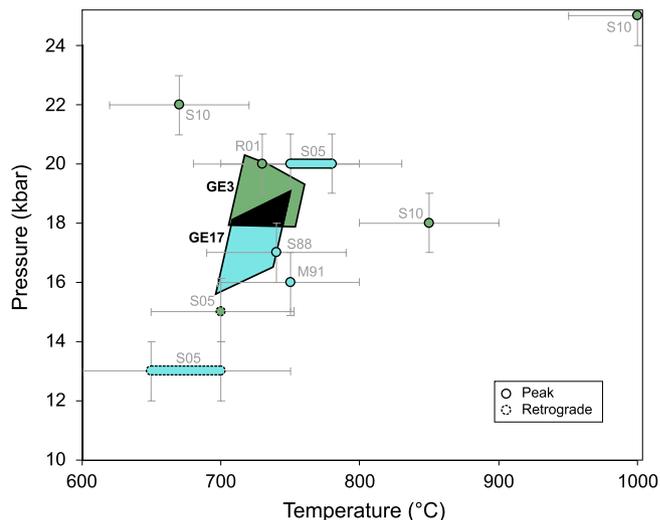


**FIGURE 11** | *P–T* results from this study (samples GE3 and GE17) plotted alongside published estimates from the Eastern Unit of the Glenelg inlier: S88 = Sanders 1988; M91 = Manning and Bohlen 1991; R01 = Rawson, Carswell, and Smallwood 2001; S05 = Storey, Brewer, and Temperley 2005; S10 = Sajeev et al. 2010. Uncertainties are assumed to be ±1 kbar and ±50°C. Blue shading denotes estimates from felsic lithologies and green shading denotes mafic lithologies. The black polygon denotes the region of overlap between the two estimated *P–T* fields from this study.

changes in phase modes. The measured modes for the observed assemblage are highlighted by the red lines, and are concentrated around 16 kbar. Clinopyroxene and kyanite modes decrease down pressure, while plagioclase, garnet and muscovite modes increase. Given the petrographic observations outlined above of resorbed kyanite surrounded by plagioclase-muscovite coronae, embayed omphacite and euhedral garnet (Figure 5f,g), the phase equilibrium modelling suggests that the observed assemblage was attained following decompression from higher pressure (i.e., more omphacite and kyanite rich) conditions, in agreement with the findings of Sanders (1988). Plagioclase is notably pressure sensitive in this region of $P$–$T$ space, decreasing from the observed 61 vol.% at 16 kbar to 0 vol.% at 18.5 kbar (Figure 10b). Although petrographic observations indicate that some plagioclase is retrograde in nature (e.g., forming coronae around kyanite), the observation of straight grain boundaries with garnet and omphacite indicates that plagioclase was present at peak conditions. Therefore, we consider it unlikely that the sample reached higher pressure conditions than 18.5 kbar (or up to 19 kbar at the highest-$T$ part of the assemblage stability range; red polygon on Figure 10a). The agreement between modelled and measured phase modes at ~16 kbar and 730°C suggests that the sample experienced up to ~2.5 kbar of decompression from the peak pressure to the preserved assemblage. This estimate is consistent with the 2 kbar estimate for decompression by Sanders (1988) from analysis of a similar felsic gneiss from Glenelg. Quantification of the total decompression based on the observed vol.% of coronae structures could potentially provide an estimate of the pressure change. However, this is not attempted because of the partial textural equilibration observed in the sample (e.g., euhedral garnet grains in Figure 5b,g, which are increasing in mode during decompression).

The peak conditions for the mafic eclogite and felsic gneiss overlap at ~18–19 kbar and 700°C–750°C (Figure 11). Analysis of microstructures and evolving phase modes in the felsic gneiss suggests partial retrograde re-equilibration occurred at lower-pressure conditions of ~16 kbar. The combined $P$–$T$ field overlaps with and further reinforces the $P$–$T$ range for peak eclogite-facies metamorphism from previous studies (16–20 kbar and 730°C–780°C; Sanders 1988; Manning and Bohlen 1991; Rawson, Carswell, and Smallwood 2001; Storey, Brewer, and Temperley 2005), with the exception of the estimates of Sajeev et al. (2010), which yielded an outlier result.

## 7 | Tectonic Setting of Eclogite Formation

We now turn our attention to the tectonic settings in which the above $P$–$T$ conditions (~18–19 kbar and 700°C–750°C) could have been attained within the context of the timing of eclogite formation and partial exhumation at c. 1.2–0.9 Ga. As discussed above, the tectonic setting of the protolith of the mafic components within the Glenelg inlier is uncertain. However, the time gap between formation (c. 2 Ga Brewer et al. 2003; Bird et al. 2023) and eclogite-facies metamorphism (c. 1 Ga) means that this material must have been tectonically incorporated into continental crust at some point prior to eclogite-facies metamorphism if it was originally oceanic or if the protoliths originally intruded into continental material. In this environment, the metamorphic conditions encompass

a range of possible tectonic settings, including continental underthrusting and thickened continental lower crust. Therefore, we here discuss additional constraints on eclogite-forming settings by considering the Neoproterozoic sedimentary rocks surrounding the Glenelg inlier (Figure 1), whose source area is the Grenville orogen (Brook, Brewer, and Powell 1976; Rainbird et al. 2017; Rainbird, Hamilton, and Young 2001; Krabbendam, Strachan, and Prave 2022; Krabbendam et al. 2017; Krabbendam, Prave, and Cheer 2008).

The purpose of this section is to build an understanding of the depositional environment and geometry of the Grenville orogen through consideration of the sedimentology and stratigraphy of the successions, and their deposition ages, paleocurrents and spatial distributions. We begin by describing the sedimentary successions from west to east (Figure 1). The units are described with respect to the three major tectonostratigraphic divisions in northwest Scotland (Johnstone, Smith, and Harris 1969): the Caledonian foreland (and Kishorn nappe), the Moine nappe, and the Sgurr Beag nappe. The Glenelg eclogite is located to the east of the Caledonian foreland units, is tectonically juxtaposed against the Morar Group in the lower portion of the Moine nappe and is to the west of the remainder of the units deformed during the Caledonian orogeny (Figure 1). All paleocurrent directions are given in present-day co-ordinates, with the original studies having removed the effects of Caledonian folding and tilting. These data are summarised in Figure 12 and Table S7.

### 7.1 | Caledonian Foreland and Kishorn Nappe (Lewisian Basement, Stoer Group, Sleat Group and Torridon Group)

The Caledonian foreland consists of Archean to Paleoproterozoic basement gneiss of the Lewisian Gneiss Complex overlain unconformably by a thick succession (up to ~10 km) of siliciclastic rocks belonging to the Stoer Group, Sleat Group and Torridon Group (Stewart 2002; Figure 12). The Torridon Group overlies both the Sleat Group and Lewisian basement and consists of a >6 km succession (unit A, Figure 12) of medium- to coarse-grained arkosic sandstone with granule-pebble lags and rare muddy intervals. The Torridon Group is characterised by an overall upward-fining succession with stacked cross-stratified 'sheets', commonly featuring soft-sediment deformation structures and consistent southeast paleocurrent directions (McMahon and Davies 2020). See Table S6 for detailed unit descriptions and both Figure 12 (blue arrows) and Table S7 for paleocurrent orientation data.

The Stoer Group is a 2 km-thick succession of limited spatial extent, composed mainly of arkosic sandstone and more minor conglomerate (Stewart 1969, 2002). The unit is bounded below by the Lewisian basement and above by an angular disconformity with the Torridon Group. The Stoer Group is not discussed further as it is thought to record localised sediment accumulation influenced by basement topography and not the regional sedimentation patterns of interest.

The Sleat Group is restricted to the area west of Glenelg, in the hanging wall of the Kishorn thrust (Figure 1). The ∼3.5 km-thick succession (unit B, Figure 12) consists mainly of interbedded sandstone and mudstone displaying sedimentary structures consistent with deposition within a mixed shallow marine and tidal-fluvial setting (Krabbendam et al. 2017; Table S6). Unimodal paleocurrent directions are to the northeast and southeast, while bimodal currents are oriented northeast-southwest (blue arrows, Figure 12; Sutton and Watson 1964).

## 7.2 | Moine Nappe (Morar Group)

The Moine nappe consists of the Morar Group, which is a uniform 6 to 9 km-thick succession of subarkosic psammite with minor (semi)pelitic and pebbly intervals (Bonsor et al. 2010; Krabbendam et al. 2017; Table S6). A lower unit (units D and F, Figure 12) consists of cross-bedded fluviatile psammite with abundant soft-sediment deformation features. An upper unit (units E and G) consists of interbedded finer-grained psammite and semipelite, with (semi)pelitic intervals. Heterolithic bedforms in the upper unit are consistent with deposition within a tidally influenced marine setting (Krabbendam, Prave, and Cheer 2008; Figure 12). Paleocurrent orientation data generally suggest northeast flow within fluviatile channel facies and bimodal northwest-southeast flow within tidally influenced facies (Figure 12; Glendinning 1989; Bonsor and Prave 2008; Bonsor et al. 2010; Krabbendam, Prave, and Cheer 2008).

## 7.3 | Sgurr Beag Nappe (Glenfinnan Group and Loch Eil Group)

The Sgurr Beag nappe consists of deformed pelitic gneiss (Glenfinnan Group, unit H) and psammite plus quartzite (Loch Eil Group, unit I) (Roberts et al. 1987; Figure 12). Sedimentary structures are rarely preserved in the Glenfinnan Group and are more prominent in the Loch Eil Group where they include both cross bedding and wave ripples. Pelitic rocks of the Glenfinnan Group are observed to pass both laterally and vertically into psammitic rocks of the Loch Eil Group. The combined thickness of the strata may be in the range 5 to 9 km (Holdsworth, Strachan, and Harris 1994; Strachan 1985). The dominantly pelitic Glenfinnan Group is likely to have been deposited in a shallow marine setting, while components of the dominantly psammitic Loch Eil Group (e.g., thin interbeds and bimodal flow indicators) imply a shallower, tidally influenced setting (Strachan 1985). Strachan (1986) reported dominantly north-northeast flow directions with occasional south-southwest flow reversals (Figure 12).

## 7.4 | Deposition Ages

Numerous U-Pb detrital zircon geochronology data are available for metasedimentary units from the three tectonostratigraphic divisions described above (Figure 12). U-Pb zircon age distributions for these units were compiled by Krabbendam,

Strachan, and Prave (2022) and show major peaks at c. 1750 and 1650 Ma, with minor peaks between c. 1500 and 1200 Ma (Friend et al. 2003; Cawood et al. 2004; Kirkland, Strachan, and Prave 2008; Krabbendam et al. 2017; Cawood et al. 2015). Single (youngest) detrital zircon ages are shown on the stratigraphic columns in Figure 12. These ages are not always in stratigraphic order, indicating that this dataset is an incomplete and/or reworked record of deposition. However, plotting of the youngest age data overall (youngest single ages and peaks) in the kernel density plot in Figure 8 reveals that the sedimentary successions were broadly deposited in the interval c. 1.1–0.9 Ga. In the Sgurr Beag nappe, a minimum depositional age of 870 Ma is constrained by the age of the intruding West Highland Granitic Gneiss (Figure 12; Rogers et al. 2001). This depositional age range overlaps with the timing of eclogite-facies metamorphism in the Glenelg inlier (Figure 8), which was later emplaced within this sedimentary sequence. This emplacement was by west-directed thrusting during Caledonian times, meaning that the eclogite must have formed at depth in a location overlain by the more easterly of these units (discussed in more detail below). The environment of deposition of these sedimentary rocks therefore helps to further constrain the tectonic setting in which the eclogite formed.

## 7.5 | Basin-Scale Characteristics

The sedimentary successions in the Caledonian foreland and Moine nappe have previously been interpreted as laterally correlative on account of their shared sedimentological and detrital age characteristics (Krabbendam, Prave, and Cheer 2008), and they are referred to collectively as the 'Wester Ross Supergroup' after Krabbendam, Strachan, and Prave (2022). The Sgurr Beag nappe units ('Loch Ness Supergroup' of Krabbendam, Strachan, and Prave 2022) are apparently slightly younger and feature more shallow marine lithofacies. We agree with the interpretation of Krabbendam, Strachan, and Prave (2022) that the Wester Ross and Loch Ness Supergroups accumulated within a single evolving basin and not within compartmentalised 'sub-basins' as previously proposed (e.g., Glendinning 1989; Soper, Harris, and Strachan 1998).

The available sedimentological and detrital zircon data reveal the following key characteristics among the successions in the Caledonian foreland and overlying nappes, which we will use below to infer the large-scale depositional setting: (1) up to ∼10 km of stratigraphy dominated by cross-bedded fluviatile to shallow marine sandstone/psammite; (2) northeast to southeast-oriented unimodal paleocurrents; and (3) all units contain a significant Paleoproterozoic detrital zircon component.

To understand the depositional setting, we need to estimate how wide the basin could have been. The total present-day width of these outcrops is ∼100 km (Figure 1). However, these units have been affected by telescoping during Caledonian thrusting. Butler (1986) estimated shortening of ∼65% in the Moine nappe, and we assume the same degree of strain within the Sgurr Beag nappe. The measured <50 km width of Moine nappe and <60 km width of the Sgurr Beag nappe
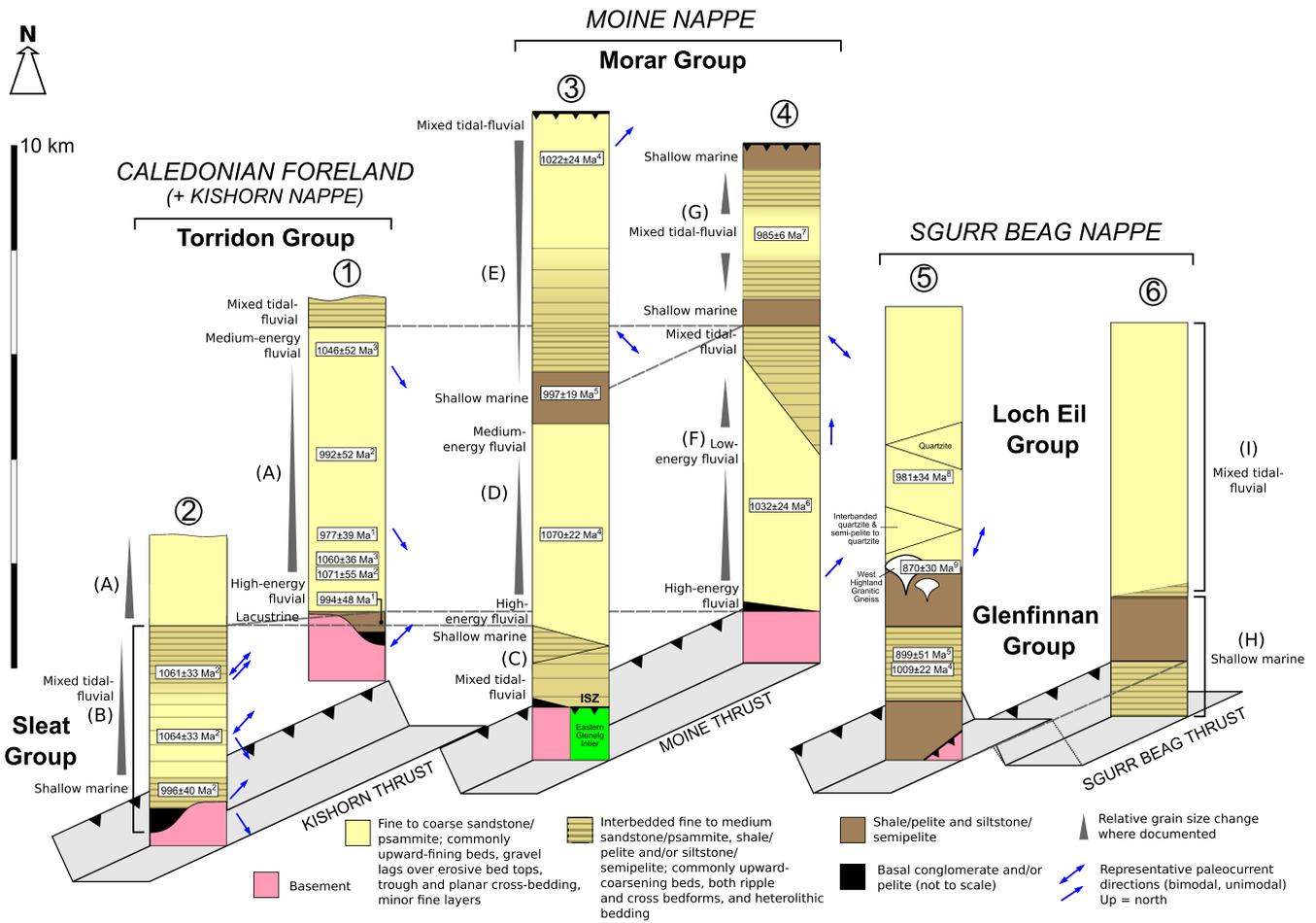
**FIGURE 12** | Schematic diagram showing tectonostratigraphic elements of the northern segment of the Caledonian orogen in northwest Scotland prior to Caledonian deformation, annotated with detrital geochronology estimates, paleocurrent directions (blue arrows) and relative grain-size changes. Incipient thrust faults dip southeast. Representative, vertically scaled stratigraphic columns are modified from published literature; see Table S6 for descriptions of labelled units. The Glenelg inlier is depicted by the green box in column three below the Inverinate shear zone (ISZ). Column numbers correspond to locations shown in Figure 1. Columns are labelled with Rb-Sr whole-rock diagenetic ages from Turnbull, Whitehouse, and Moorbath (1996) (superscript 1) and maximum deposition ages from U-Pb detrital zircon analyses: 2–Krabbendam et al. 2017; 3–Rainbird, Hamilton, and Young 2001; 4–Kirkland, Strachan, and Prave 2008; 5–Cawood et al. 2015; 6–Friend et al. 2003; 7–Peters 2001; 8–Cawood et al. 2004; 9–Rogers et al. 2001. The intrusive age of the West Highland Granitic Gneiss is also shown on column five as it places a minimum age constraint on deposition of the Neoproterozoic sediments.

correspond to 'unfolded' widths of up to 77 and 92 km, respectively. Undeformed sedimentary rocks overlying the Caledonian foreland have a width of up to ~30 km, yielding a collective total of ~200 km. Total displacement across the Moine thrust is probably on the order of 100 km (Elliott and Johnson 1980). Displacement across the Sgurr Beag thrust is less well constrained, but we will here assume it was similar to the Moine thrust (e.g., akin to the Main Central thrust and Main Boundary thrust in the Himalayas; Yin 2006). Adding these thrust displacements to our 'unfolded' basin width gives a total of 400 km. The thrust displacements could have been larger than estimated. Alternatively, all units may not have been deposited contemporaneously and the preserved record may represent different snapshots of a basin evolving spatially through time, in which case the estimate above is an upper bound. Regardless of which of these considerations dominates, it is clear that the basin must have had a width on the order of hundreds of kilometres.

## 7.6 | Interpreted Depositional Setting

The sedimentary setting that can account for all of the observed characteristics is deposition in a filled continental foreland basin. Continental foreland basins are characterised by several kilometre-thick strata of clastic sediment, widths of up to ~350 km (DeCelles and Giles 1996; Catuneanu, Miall, and Sweet 1997; Horton and DeCelles 1997; Grimaud et al. 2020) and commonly have shallow water to terrestrial sedimentary facies throughout (DeCelles 2011). Depositional settings that have previously been proposed for the sedimentary successions include a foreland basin (Rainbird, Hamilton, and Young 2001; Kinnaird et al. 2007; Bonsor and Prave 2008; Bonsor et al. 2010; 2012; Krabbendam, Prave, and Cheer 2008; Krabbendam et al. 2017) or an extensional basin (Williams and Foden 2011; Stewart 2002; Soper, Harris, and Strachan 1998; Glendinning 1989) including the post-rift thermal sag phase (Nicholson 1994). An extensional basin is unlikely as they are considerably narrower than the basin width we estimate

above, with individual fault-bounded basin widths similar to the thickness of the seismogenic layer (Copley and Woodcock 2016). Furthermore, extensional basins exhibit several features in the sedimentary architecture that are not observed, such as rapid lateral and vertical facies changes associated with fault-controlled changes in accommodation space, volcanic, evaporitic and lacustrine horizons and variable flow directions (Krabbendam, Prave, and Cheer 2008; Matenco and Haq 2020). Post-rift thermal subsidence would be unable to generate the >6 to 9 km of accommodation space for the amounts of thinning that could be compatible with the deposition of shallow-water sedimentary facies (McKenzie 1978; Middleton 1989).

Taken together, the presented sedimentological information indicate that the Scottish Neoproterozoic successions accumulated in a foreland basin at c. 1.1 to 0.9 Ga, with sediment derived from the Grenville orogen (e.g., Rainbird, Hamilton, and Young 2001; Kinnaird et al. 2007; Bonsor and Prave 2008; Bonsor et al. 2010; 2012; Krabbendam, Prave, and Cheer 2008; Krabbendam et al. 2017; Krabbendam, Strachan, and Prave 2022). As peak eclogite formation and partial exhumation (c. 1.1–0.9 Ga; Figure 8) coincided with sedimentation, we interpret the Glenelg inlier to have reached eclogite-facies conditions beneath the foreland basin adjacent to the Grenville mountain range. We discuss the implications of this tectonic interpretation in more detail below with respect to paleocurrent directions and paleoreconstructions, after first examining the viability of forming eclogites in this setting.

## 8 | Discussion

### 8.1 | Viable Eclogite-Forming Settings

Our analysis above indicates that the Glenelg eclogites formed beneath the foreland basin adjacent to the Grenville mountain belt, rather than within an 'arm' of the range (e.g., Strachan et al. 2020; Bird et al. 2023). We must now establish the mechanism by which an eclogite with peak conditions of up to 19 kbar (68 km depth, assuming 2800 kg/m$^3$) and 750°C could form in this tectonic setting. We consider two possibilities and assess their strengths and weaknesses in turn below: (1) a foreland undergoing thick-skinned deformation and (2) closure of an ocean basin. We do not explore a third possibility that the eclogite formed at the base of ~70 km-thick foreland crust in thermal steady state because this scenario is made unlikely by (1) requiring foreland crust thicker than is observed in any stable continental regions at the present day (by ≥10 km) and (2) preserved zonation in garnet grains (Figure 4), implying limited time spent equilibrating at peak conditions.

#### 8.1.1 | Thick-Skinned Foreland Deformation

One option for the formation of the Glenelg eclogite involves metamorphism at the base of thick orogenic foreland, and subsequent partial exhumation (Figure 13a). Deformation is a necessary prerequisite for causing pressure and temperature conditions
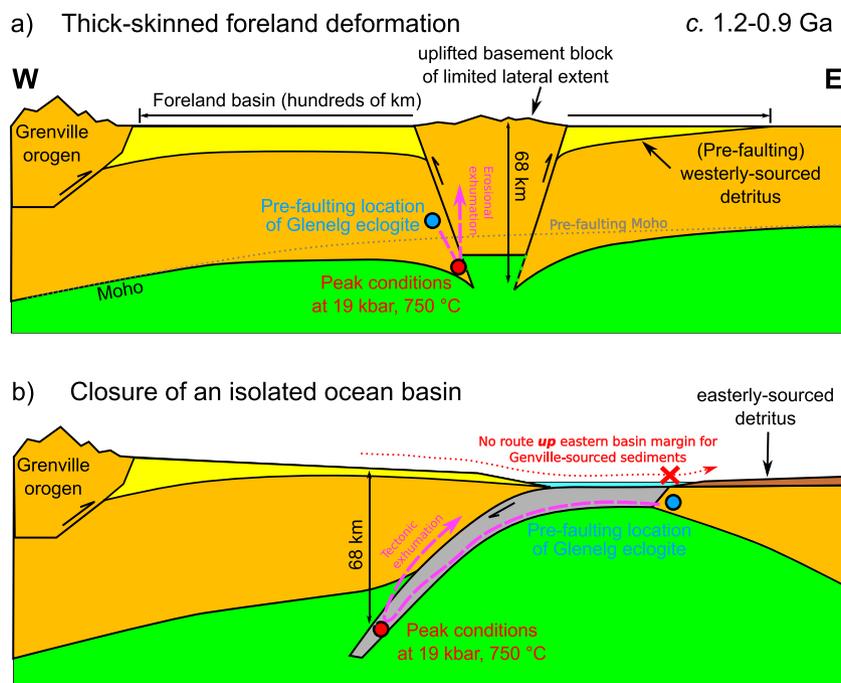


**FIGURE 13** | Possible tectonic settings for the Glenelg eclogite prior to final exhumation during the Caledonian orogeny. (a) Foreland setting analogous to present-day 'pop-up' structures, such as the Shillong Plateau in Himalayan foreland (Chen and Molnar 1990) and the San Rafael block in the Andean foreland (Olivar et al. 2023). (b) Closing oceanic basin analogous to the incipient closure of the South Caspian basin at the present day (Jackson et al. 2002). Given the structural setting of the eclogite and the Caledonian kinematics, the bulk of the Morar, Loch Eil and Glenfinnan Group metasediments were deposited to the east of the Glenelg eclogite, and the unmetamorphosed Torridon Group to the west (present-day coordinates; Figure 1).

to significantly evolve and occurs at the present day in nominally 'stable' regions in the forelands of several orogens, including the North and South American Cordillera, Himalayas, Western Alps and Pyrenees (Lacombe and Mouthereau 2002). In these regions, deformation is often visible at the surface by topographic highs formed of uplifted basement and at depth by seismicity throughout the thickness of the crust (Chen and Molnar 1990; Mitra et al. 2005; Wimpenny 2022). Basement uplifts in active ranges include the Shillong Plateau in the Himalayan foreland in India (Chen and Molnar 1990), the Wind River uplift in the Laramide foreland in Wyoming, USA (Smithson et al. 1979) and the San Rafael Block in the Andean foreland in Argentina (Olivar et al. 2023). Seismological and geodetic results show that the uplift of such features is often by slip on steeply dipping reverse faults that penetrate the entire seismogenic layer, forming basement 'pop-ups' (Chen and Molnar 1990; Wimpenny 2022). This deformation occurs in response to the compressive force transmitted through the foreland by an adjacent mountain range (Lacombe and Mouthereau 2002; Copley and Woodcock 2016; Wimpenny 2022). One possible scenario for the formation of the Glenelg eclogites is therefore burial and heating at the base of a thick foreland crust, in the footwall of such thrust faults, with final exhumation occurring considerably later, during the c. 470–420 Ma Caledonian orogeny.

### 8.1.2 | Closure of an Isolated Ocean Basin

A second possibility involves the closure of a minor ocean basin, separate from the closure of the main Mirovoi Ocean (Cawood and Pisarevsky 2017), to form the Grenville orogen (Figure 13b). Such a situation would be analogous to the present-day incipient or recent closure of the South Caspian basin and the subducted isolated ocean basin that now forms the Hindu Kush deep seismic zone (Jackson et al. 2002; Lister et al. 2008; Mellors et al. 2012). In this context, eclogite-facies conditions could be achieved in the usual situation of deep underthrusting of continental margin material attached to an oceanic slab and exhumation following slab break-off.

### 8.1.3 | Sedimentary Signatures of the Alternative Settings

We distinguish between these alternatives based upon their sedimentary signatures, before demonstrating the thermal viability of our preferred model. In the case of thick-skinned foreland deformation, the sedimentary architecture would represent a foreland basin, containing individual, spatially limited, basement uplifts. Sedimentary routing systems commonly both predate these uplifts and are diverted around their limited along-strike extents (e.g., the Shillong Plateau in the Himalayan foreland Najman et al. 2016). The sedimentary record therefore records a wide region with the same sediment source and same broad transport direction, containing small regions of nondeposition that would leave little sedimentary record. In the Grenville context, this depositional setting would be dominated by spatially extensive sediments transported broadly eastwards, away from the orogen, and sharing a common source (Figure 13a). If deposited on continental crust (as underlies Scotland), shallow-water facies will dominate, as in present-day foreland basins which fill as they form. The resulting geological

record of this setting therefore resembles that forming in northwest Scotland at the time of metamorphism of the Glenelg eclogite.

In the case of an isolated ocean basin, the sedimentary depositional setting would include a topographically low sediment barrier, and feature both shallow- and deep-water facies (Figure 13b; e.g., the South Caspian or Black Sea at the present day, which are on the order of kilometres deep). This barrier would prevent sediments from being transported across it, due to their inability to be transported up the far side of the basin (Figure 13b). Therefore, in contrast to the foreland basin setting described above, the sediments on the far side of the closing ocean basin would not be sourced from the Greville orogen and would instead be sourced from spatially separate sediment routing systems on the far side of the basin (dark brown in Figure 13b). The overall shallow-water facies of the Morar, Glenfinnan, and Loch Eil Groups precludes them having been deposited in the deep water of such a basin itself (i.e., pale blue in Figure 13b), and the easterly directed sedimentary system precludes them from having been deposited further east than such a basin (i.e., dark brown in Figure 13b).

The structural setting of the Glenelg eclogite and the kinematics of the Caledonian deformation show that the bulk of the Morar, Loch Eil and Glenfinnan Group metasediments were deposited to the east of the Glenelg eclogite, and the Torridon Group was deposited to the west (present-day co-ordinates; Figure 1). In either model, the Torridon Group would represent deposition on the Grenville
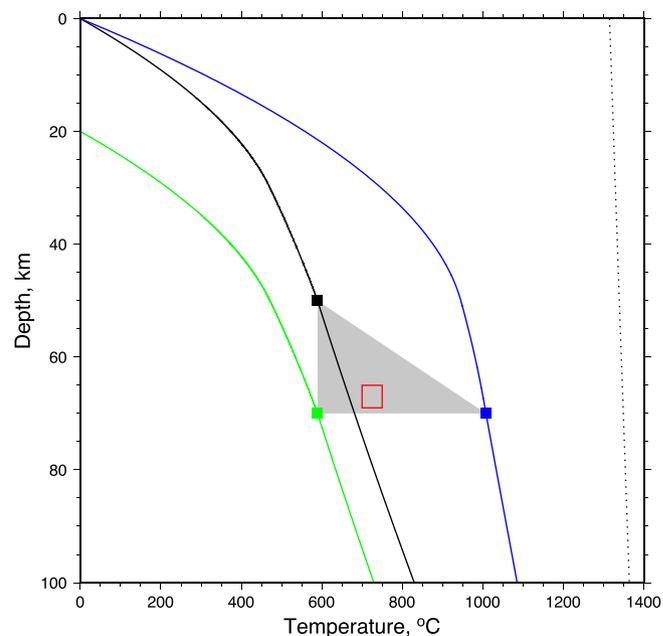


**FIGURE 14** | Model of the thermal evolution of our proposed tectonic setting for the Glenelg eclogite. The black line is a steady-state geotherm for a 50 km-thick continental crust, calculated using the parameters described in the text. The green line is the geotherm resulting from instantaneous overthrusting of 20 km of crust (i.e., downward advection of the black line). The blue line is the steady-state geotherm following thermal re-equilibration (with 70 km-thick crust) without erosion. The filled squares mark the Moho position. The grey polygon covers the likely range of transient peak conditions in the lower crust. See text for detailed explanation. The dashed black line is an isentrope for a potential temperature of 1315°C.

piedmont (left-hand side of Figure 1), so it has limited use in distinguishing the tectonic setting. However, given the record of only easterly directed sedimentation and shallow-water facies in the Morar, Loch Eil and Glenfinnan Groups, the sedimentary record in northwest Scotland is only consistent with a foreland basin setting punctuated by basement uplifts of limited lateral extent, beneath which the Glenelg eclogite could form.

## 8.2 | Thermal Viability of Proposed Setting

As the proposed thick-skinned tectonic setting is novel, we here test the viability of reaching eclogite-facies $P$–$T$ conditions in this setting. We show below (Figure 14) that this setting is thermally viable, which should not be taken as a reason why this model is correct; both alternatives are thermally viable, and it is only the other, independent evidence discussed above that demonstrates the foreland habitat of the Glenelg eclogite.

The estimated width of the Grenville foreland basin (on the order of hundreds of kilometres; see above) implies a foreland elastic thickness towards the upper end of those observed at the present day (e.g., $\geq$25 km, as is the case for the $\geq$200 km-wide Himalayan foreland basin in India; Maggi et al. 2000; McKenzie, Yi, and Rummel 2015). Such locations generally correlate with regions of past high-grade metamorphism and thick lithosphere (Jackson et al. 2008), consistent with the presence of the amphibolite- to granulite-facies Lewisian basement now exposed at the surface in northwest Scotland. Crustal thicknesses in plate-like continental interiors (e.g., India) are mostly 40–50 km but can be up to 60 km in some regions (e.g., Finland; Korsman et al. 1999). The combination of $P$–$T$ estimates from mantle xenoliths, estimates of heat production and transport, seismological estimates of lithosphere thickness and thermal models fitting these observations imply steady-state Moho temperatures beneath Precambrian shields of $\sim$500°C to over 650°C (McKenzie, Jackson, and Priestley 2005; Jackson et al. 2008). Disruption of this steady-state geotherm by horizontal shortening, vertical thickening and the associated heating in the foreland of a mountain belt could result in the $P$–$T$ conditions we have estimated above for burial of $\geq$10–30 km, for initial crustal thicknesses of 40–60 km or less if the downwards motion due to foreland flexure is also taken into account. Such a pressure increase is comparable to the effects of 10–20 km of slip on the faults bounding the southern margin of the Shillong Plateau in the Himalayan foreland (Mitra et al. 2018). Such thickening would result in heating because of the increased amount of radiogenic heating within the thicker crustal column (i.e., a given concentration of heat-producing elements distributed through thicker crust) and diffusion of heat from the exhuming hangingwall, so the temperatures achieved by the Glenelg eclogites could be attained. Subsequent thrusting in Caledonian times could then exhume these rocks to the present-day surface.

We can further test the thermal viability of this tectonic setting by constructing a simple numerical model to illustrate the $P$–$T$ conditions that would result. In Figure 14, the black line shows a typical steady-state geotherm for a continental interior, with 50 km crust, radiogenic heating of 1.5 μW/m$^3$ in the upper 30 km of the crust and 0.2 μW/m$^3$ in the lower crust and a Moho heat flux of 13 mW/m$^2$ (Gruber et al. 2021; Rudnick

and Fountain 1995; Podugu et al. 2017; McKenzie, Jackson, and Priestley 2005; Jaupart et al. 1998). These parameters result in a lithosphere thickness of 200 km, for a mantle potential temperature of 1315°C. We use a conductivity of 2.5 W/mK in the crust and the temperature-dependence suggested by McKenzie, Jackson, and Priestley (2005) in the mantle. The filled square marks the Moho. The green line shows the geotherm that would result from the instantaneous overthrusting of 20 km of crust, showing only the temperature in the footwall of the thrust. This geotherm is the same as the black one but transposed downwards by 20 km. The blue line shows the geotherm that would result from eventual re-equilibration of the temperatures, in the absence of erosion, and keeping the lithosphere thickness unchanged from the green curve (i.e., the steady-state situation with the new, greater, crustal thickness). The grey polygon shows the region of depth-temperature space between the Moho conditions in these steady-state models, which therefore covers the region where evolving geotherms could reach peak conditions in the lower crust.

The green curve is unlikely to be achieved in reality because tens of kilometres of thrusting is not instantaneous. The blue line is equally unlikely because erosion acts to reduce the thickness of 70 km-thick crust before steady-state can be achieved. As an illustration of this concept, the characteristic thermal timescale for diffusive re-equilibration through the lithosphere is given by $\tau = l^2/\pi^2\kappa$, where $l$ is the lithosphere thickness, $\kappa$ is the thermal diffusivity ($\sim 10^{-6}$ m$^2$/s for common rock types). If $l$ is 220 km, $\tau$ is therefore on the order of hundreds of millions of years, so it is unlikely that thermal re-equilibration can occur during the time when the crust is thick. The region in the centre of the grey polygon is therefore most likely to be sampled in this tectonic setting, with finite rates of thrusting and erosion, which is in agreement with the conditions experienced by the Glenelg eclogite (red box). Our suggested tectonic setting is therefore thermally viable.

## 8.3 | Constraints on Proterozoic Plate Reconstructions

The arguments presented above indicate that the Glenelg eclogite formed in a foreland setting and show how such a setting can viably result in the observed eclogite-facies metamorphism. We now address the constraints this conclusion places on paleore-constructions of the Grenville orogen.

The trace of the Grenville orogen is well-constrained across Canada and Scandinavia due to the vast and semicontinuous associated rock record of metamorphism and deformation over thousands of kilometres (Rivers 1997; Rivers et al. 2012; Bingen et al. 2021; Weller et al. 2021). The record in the intervening regions is sparse, and limited to the Glenelg inlier in Scotland and the Annagh Gneiss Complex in Ireland, meaning reconstructions are ambiguous between Canada and Scandinavia. Scotland is generally positioned between Scandinavia and Greenland/ northeast Canada in reconstructions (Figure 15) based upon well-established basement correlations with Laurentia (Park 1995; Wheeler et al. 2010; Park 2022) and paleomagnetic data (Darabi and Piper 2004; Borradaile and Geneviciene 2008). The Glenelg eclogite has been used to propose the existence of a third 'arm'
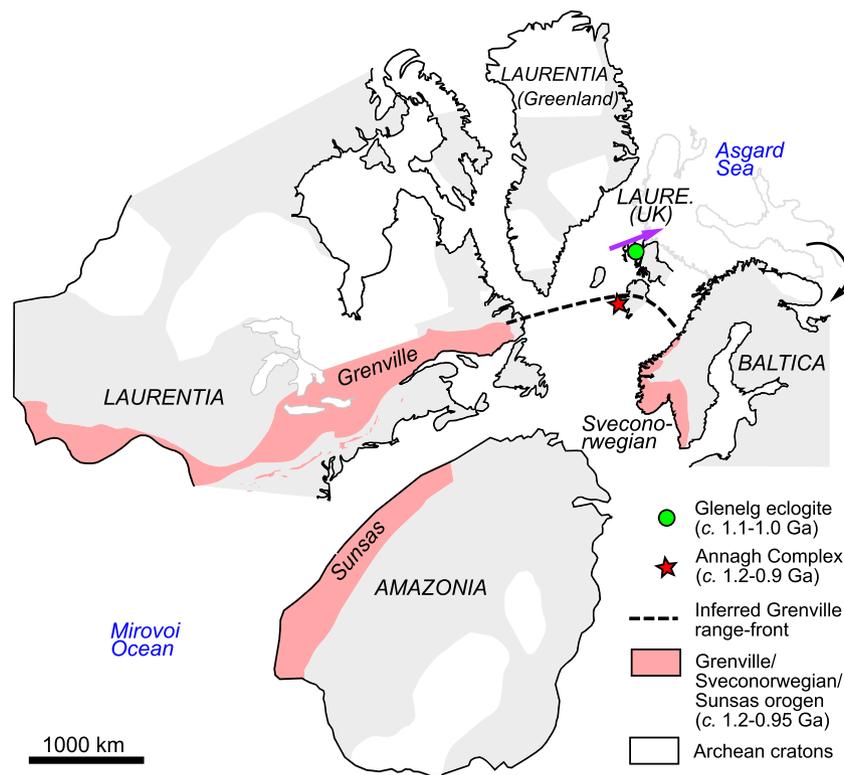
*Journal of Metamorphic Geology*, 2024

**FIGURE 15** | Paleoreconstruction for Laurentia, Baltica and Amazonia at c. 1 Ga from Cawood et al. (2007). As per Cawood et al. (2007), the continents are shown separated for clarity, even though they formed the supercontinent Rodinia. The black arrow denotes Baltica's clockwise rotation from its orientation before c. 1.12 Ga (grey outline Buchan et al. 2000; Salminen, Elming, and Layer 2023).

to the orogen, perpendicular to the trend of the range in Canada (Strachan et al. 2020; Bird et al. 2023), in order to reconcile the location of Scotland with an eclogite presumed to have formed proximal to a suture zone (i.e., within the interior of the deformation belt).

The broad position of Scotland at c. 1 Ga, adjacent to the exposed Archean rocks of southern Greenland (Park 1995), is shown on Figure 15, and our results are interpreted in this context. The northeast to southeast paleocurrents shown on Figure 12 are likely to represent a combination of along- and across-strike flow within the foreland basin. Previous studies on the Grenville foreland in Canada have suggested dominantly orogen-parallel trunk rivers (Rainbird, Hamilton, and Young 2001, Rainbird et al. 2017). In Scotland, although previous studies have similarly suggested along-strike flow (Rainbird, Hamilton, and Young 2001; Kinnaird et al. 2007; Krabbendam, Prave, and Cheer 2008; Krabbendam et al. 2017), the range of northeast to southeast paleocurrents (Figure 12) mean that we instead prefer a setting involving flow both perpendicular and parallel to the orogen over a wide area. This situation places the Grenville belt broadly to the west in the present reference frame of Scotland (Figure 15).

As shown in Figure 15 and taking into account the poorly constrained orientation of Scotland in these reconstructions due to subsequent relative rotations, broadly eastward-directed paleocurrents (i.e., in the direction shown on Figure 15) are consistent with sediment sources from known exposures of the Grenville orogen (e.g., c. 1.65 Ga Trans-Labrador batholith;

Rainbird, Hamilton, and Young 2001; Krabbendam et al. 2017), flowing parallel to, and away from, the mountain belt. Our suggested foreland position is therefore consistent with other information on the geometry of the Grenville orogen and implies that there was no third 'arm' of the orogen running through northern Scotland. Importantly, this conclusion also reconciles the absence of plentiful Grenville-aged metamorphic rocks in this region, as would be expected to have resulted from an orogen of this scale. The Grenville range-front may have run between the outcrops of the Glenelg inlier and the Annagh Gneiss Complex (Figures 1 and 15). Furthermore, the concept of significant convergence between Laurentia and Baltica at this time, as required by the third arm of the Grenville orogen, is at odds with paleomagnetic data which indicate the region was instead characterised by opening of the 'Asgard' sea between Greenland and Scandivania at this time (Figure 15; Salminen, Elming, and Layer 2023; Cawood et al. 2010; Buchan et al. 2000; Patchett, Bylund, and Upton 1978). Overall, our new tectonic interpretation of the Glenelg eclogite simplifies the geometry of the Grenville belt in the British Isles and is consistent with metamorphic, sedimentological and paleomagnetic constraints from Scotland.

## 9 | Conclusions

We have demonstrated that eclogite-facies metamorphism recorded in the Glenelg inlier (~18–19 kbar and 700°C–750°C, culminating at c. 1.1–1.0 Ga) occurred beneath a foreland basin beyond the range-front of the Grenville orogenic belt. Our

results underscore the importance of combining multiple lines of evidence from the rock record when interpreting the tectonic significance of metamorphic rocks, particularly where outcrop is limited. There may well be fewer suture zones preserved in the geological record than previously thought.

## Conflicts of Interest

The authors declare no conflicts of interest.

## References

Ashley, K. T., J. R. Thigpen, and R. D. Law. 2015. "Prograde Evolution of the Scottish Caledonides and Tectonic Implications." *Lithos* 224-225: 160–178. https://doi.org/10.1016/j.lithos.2015.03.011.

Barber, A. J. 2011. "The Structure of the Glenelg-Attadale Lewisianoid Inlier and Its Relationship to the Moine Thrust Zone." *Scottish Journal of Geology* 47, no. 2: 113–132. https://doi.org/10.1144/0036-9276/01-427.

Barr, D., R. E. Holdsworth, and A. M. Roberts. 1986. "Caledonian Ductile Thrusting in a Precambrian Metamorphic Complex: The Moine of Northwestern Scotland." *GSA Bulletin* 97, no. 6: 754–764. https://doi.org/10.1130/0016-7606(1986)97<754:CDTIAP>2.0.CO;2.

Bingen, B., G. Viola, C. Müller, J. Vander Auwera, A. Laurent, and K. Yi. 2021. "The Sveconorwegian Orogeny." *Gondwana Research* 90: 273–313. https://doi.org/10.1016/j.gr.2020.10.014.

Bird, A., M. Thirlwall, R. A. Strachan, I. L. Millar, E. D. Dempsey, and K. Hardman. 2023. "Eclogites and Basement Terrane Tectonics in the Northern Arm of the Grenville Orogen, NW Scotland." *Geoscience Frontiers* 14, no. 6: 101668. https://doi.org/10.1016/j.gsf.2023.101668.

Bonsor, H. C., and A. R. Prave. 2008. "The Upper Morar Psammite of the Moine Supergroup, Ardnamurchan Peninsula, Scotland: Depositional Setting, Tectonic Implications." *Scottish Journal of Geology* 44, no. 2: 111–122. https://doi.org/10.1144/sjg44020111.

Bonsor, H. C., R. A. Strachan, A. R. Prave, and M. Krabbendam. 2010. "Fluvial Braidplain to Shallow Marine Transition in the Early Neoproterozoic Morar Group, Fannich Mountains, Northern Scotland." *Precambrian Research* 183, no. 4: 791–804. https://doi.org/10.1016/j.precamres.2010.09.007.

Bonsor, H. C., R. A. Strachan, A. R. Prave, and M. Krabbendam. 2012. "Sedimentology of the Early Neoproterozoic Morar Group in Northern Scotland: Implications for Basin Models and Tectonic Setting." *Journal of the Geological Society* 169, no. 1: 53–65. https://doi.org/10.1144/0016-76492011-039.

Borradaile, G. J., and I. Geneviciene. 2008. "Late Proterozoic Reconstructions of North-West Scotland and Central Canada: Magnetic Fabrics, Paleomagnetism and Tectonics." *Journal of Structural Geology* 30, no. 12: 1466–1488. https://doi.org/10.1016/j.jsg.2008.07.009.

Brewer, T. S., C. D. Storey, R. R. Parrish, S. Temperley, and B. F. Windley. 2003. "Grenvillian Age Decompression of Eclogites in the Glenelg-Attadale Inlier, NW Scotland." *Journal of the Geological Society, London* 160: 565–574. https://doi.org/10.1144/0016-764902-061.

British Geological Survey. 2007. "Bedrock Geology UK North, 1:250 000 Scale. British Geological Survey, Keyworth, Nottingham."

Brook, M., M. S. Brewer, and D. Powell. 1976. "Grenville Age for Rocks in the Moine of North-Western Scotland." *Nature* 260, no. 5551: 515–517. https://doi.org/10.1038/260515a0.

Buchan, K. L., S. Mertanen, R. G. Park, et al. 2000. "Comparing the Drift of Laurentia and Baltica in the Proterozoic: the Importance of Key Palaeomagnetic Poles." *Tectonophysics* 319, no. 3: 167–198. https://doi.org/10.1016/S0040-1951(00)00032-9.

Butler, R. W. H. 1986. "Structural Evolution in the Moine of Northwest Scotland: A Caledonian Linked Thrust System?." *Geological Magazine* 123, no. 1: 1–11. https://doi.org/10.1017/S0016756800026492.

Catuneanu, O., A. D. Miall, and A. R. Sweet. 1997. "Reciprocal Architecture of Bearpaw T-R Sequences, Uppermost Cretaceous, Western Canada Sedimentary Basin." *Bulletin of Canadian Petroleum Geology* 45, no. 1: 75–94. https://doi.org/10.35767/gscpgbull.45.1.075.

Cawood, P. A., A. A. Nemchin, R. A. Strachan, P. D. Kinny, and S. Loewy. 2004. "Laurentian Provenance and an Intracratonic Tectonic Setting for the Moine Supergroup, Scotland, Constrained by Detrital Zircons From the Loch Eil and Glen Urquhart Successions." *Journal of the Geological Society* 161, no. 5: 861–874. https://doi.org/10.1144/16-764903-117.

Cawood, P. A., A. A. Nemchin, R. A. Strachan, T. Prave, and M. Krabbendam. 2007. "Sedimentary Basin and Detrital Zircon Record Along East Laurentia and Baltica During Assembly and Breakup of Rodinia." *Journal of the Geological Society, London* 164: 257–275. https://doi.org/10.1144/0016-76492006-115.

Cawood, P. A., and S. A. Pisarevsky. 2017. "Laurentia-Baltica-Amazonia Relations During Rodinia Assembly." *Precambrian Research* 292: 386–397. https://doi.org/10.1016/j.precamres.2017.01.031.

Cawood, P. A., R. Strachan, K. Cutts, P. D. Kinny, M. Hand, and S. Pisarevsky. 2010. "Neoproterozoic Orogeny Along the Margin of Rodinia: Valhalla Orogen, North Atlantic." *Geology* 38, no. 2: 99–102. https://doi.org/10.1130/g30450.1.

Cawood, P. A., R. A. Strachan, R. E. Merle, et al. 2015. "Neoproterozoic to Early Paleozoic Extensional and Compressional History of East Laurentian Margin Sequences: The Moine Supergroup, Scottish Caledonides." *Geological Society of America Bulletin* 127, no. 3-4: 349–371. https://doi.org/10.1130/b31068.1.

Chen, W.-P., and P. Molnar. 1990. "Source Parameters of Earthquakes and Intraplate Deformation Beneath the Shillong Plateau and the Northern Indoburman Ranges." *Journal of Geophysical Research: Solid Earth* 95, no. B8: 12527–12552. https://doi.org/10.1029/JB095iB08p12527.

Cherniak, D. J., J. Manchester, and E. B. Watson. 2007. "Zr and Hf Diffusion in Rutile." *Earth and Planetary Science Letters* 261, no. 1: 267–279. https://doi.org/10.1016/j.epsl.2007.06.027.

Coggon, R., and T. J. B. Holland. 2002. "Mixing Properties of Phengitic Micas and Revised Garnet-Phengite Thermobarometers." *Journal of Metamorphic Geology* 20, no. 7: 683–696. https://doi.org/10.1046/j.1525-1314.2002.00395.x.

Copley, A., and N. Woodcock. 2016. "Estimates of Fault Strength From the Variscan Foreland of the Northern UK." *Earth and Planetary Science Letters* 451: 108–113. https://doi.org/10.1016/j.epsl.2016.07.024.

Crisp, L. J., A. J. Berry, A. D. Burnham, L. A. Miller, and M. Newville. 2023. "The Ti-in-Zircon Thermometer Revised: The Effect of Pressure on the Ti Site in Zircon." *Geochimica et Cosmochimica Acta* 360: 241–258. https://doi.org/10.1016/j.gca.2023.04.031.

Cutts, K. A., P. D. Kinny, R. A. Strachan, et al. 2010. "Three Metamorphic Events Recorded in a Single Garnet: Integrated Phase Modelling, In Situ LA-ICPMS and SIMS Geochronology From the Moine Supergroup, NW

Scotland." *Journal of Metamorphic Geology* 28, no. 3: 249–267. https://doi.org/10.1111/j.1525-1314.2009.00863.x.

Daly, S. 1996. "Pre-Caledonian History of the Annagh Gneiss Complex North-Western Ireland, and Correlation With Laurentia-Baltica." *Irish Journal of Earth Sciences* 15: 5–18.

Daly, S., and M. Flowerdew. 2005. "Grampian and Late Grenville Events Recorded by Mineral Geochronology Near a Basement-Cover Contact in North Mayo, Ireland." *Journal of the Geological Society, London* 162: 163–174.

Darabi, M. H., and J. D. A. Piper. 2004. "Palaeomagnetism of the (Late Mesoproterozoic) Stoer Group, Northwest Scotland: Implications for Diagenesis, Age and Relationship to the Grenville Orogeny." *Geological Magazine* 141, no. 1: 15–39. https://doi.org/10.1017/S0016756803008148.

de Capitani, C., and K. Petrakakis. 2010. "The Computation of Equilibrium Assemblage Diagrams With Theriak/Domino Software." *American Mineralogist* 95: 1006–1016.

DeCelles, P. G. 2011. "Foreland Basin Systems Revisited: Variations in Response to Tectonic Settings." *Tectonics of Sedimentary Basins*, pp. 405–426. https://doi.org/10.1002/9781444347166.ch20.

DeCelles, P. G., and K. A. Giles. 1996. "Foreland Basin Systems." *Basin Research* 8, no. 2: 105–123. https://doi.org/10.1046/j.1365-2117.1996.01491.x.

Elliott, D., and M. R. W. Johnson. 1980. "Structural Evolution in the Northern Part of the Moine Thrust Belt, NW Scotland." *Earth and Environmental Science Transactions of the Royal Society of Edinburgh* 71, no. 2: 69–96. https://doi.org/10.1017/S0263593300013523.

Ernst, W. G. 1973. "Blueschist Metamorphism and P-T regimes in Active Subduction Zones." *Tectonophysics* 17, no. 3: 255–272. https://doi.org/10.1016/0040-1951(73)90006-1.

Ewing, T. A., D. Rubatto, M. Beltrando, and J. Hermann. 2015. "Constraints on the Thermal Evolution of the Adriatic Margin During Jurassic Continental Break-up: U-Pb Dating of Rutile From the Ivrea-Verbano Zone, Italy." *Contributions to Mineralogy and Petrology* 169, no. 4: 44. https://doi.org/10.1007/s00410-015-1135-6.

Fettes, D. J., C. B. Long, R. E. Bevins, et al. 1985. "Grade and Time of Metamorphism in the Caledonide Orogen of Britain and Ireland." *Geological Society, London, Memoirs* 9, no. 1: 41–53. https://doi.org/10.1144/GSL.MEM.1985.009.01.03.

Friend, C. R. L., R. A. Strachan, and P. D. Kinny. 2008. "U-Pb Zircon Dating of Basement Inliers Within the Moine Supergroup, Scottish Caledonides: Implications of Archaean Protolith Ages." *Journal of the Geological Society* 165, no. 4: 807–815. https://doi.org/10.1144/0016-76492007-125.

Friend, C. R. L., R. A. Strachan, P. D. Kinny, and G. R. Watt. 2003. "Provenance of the Moine Supergroup of NW Scotland: Evidence From Geochronology of Detrital and Inherited Zircons From (Meta) Sedimentary Rocks, Granites and Migmatites." *Journal of the Geological Society, London* 160: 247–257. https://doi.org/10.1144/0016-764901-161.

Glendinning, N. R. 1989. "The Sedimentology of Proterozoic, Moine Rocks of West Scotland." (PhD thesis), Royal Holloway, University of London.

Green, E. C. R., R. W. White, J. F. A. Diener, R. Powell, T. J. B. Holland, and R. M. Palin. 2016. "Activity-Composition Relations for the Calculation of Partial Melting Equilibria in Metabasic Rocks." *Journal of Metamorphic Geology* 34, no. 9: 845–869. https://doi.org/10.1111/jmg.12211.

Grimaud, J. L., C. Grall, S. Goodbred, et al. 2020. "Flexural Deformation Controls on Late Quaternary Sediment Dispersal in the Garo-Rajmahal Gap, NW Bengal Basin." *Basin Research* 32, no. 5: 1242–1260. https://doi.org/10.1111/bre.12425.

Gruber, B., T. Chacko, D. G. Pearson, C. Currie, and A. Menzies. 2021. "Heat Production and Moho Temperatures in Cratonic Crust: Evidence

From Lower Crustal Xenoliths From the Slave Craton." *Lithos* 380-381: 105889. https://doi.org/10.1016/j.lithos.2020.105889.

Hoffman, P. F. 1991. "Did the Breakout of Laurentia Turn Gondwanaland Inside-Out?." *Science* 252, no. 5011: 1409–1412. https://doi.org/10.1126/science.252.5011.1409.

Holdsworth, R. E., R. A. Strachan, and G. I. Alsop. 2001. *Solid Geology of the Tongue District*. British Geological Survey.

Holdsworth, R. E., R. A. Strachan, and A. L. Harris. 1994. "Precambrian Rocks in Northern Scotland East of the Moine Thrust: The Moine Supergroup." edited by W. Gibbons, and A. L. Harris, *A Revised Correlation of Pre-Cambrian Rocks in the British Isles*, Vol. 22. Geological Society of London. https://doi.org/10.1144/SR22.3.

Holland, T. J. B. 2009. "AX: Calculate Activities of Mineral Endmembers From Chemical Analyses." https://filedn.com/lU1GlyFhv3UuXg5E9dbnWFF/TJBHpages/ax.html.

Holland, T. J. B., E. C. R. Green, and R. Powell. 2022. "A Thermodynamic Model for Feldspars in $KAlSi_3O_8$-$NaAlSi_3O_8$-$CaAl_2Si2O_8$ for Mineral Equilibrium Calculations." *Journal of Metamorphic Geology* 40, no. 4: 587–600. https://doi.org/10.1111/jmg.12639.

Holland, T. J. B., and R. Powell. 2011. "An Improved and Extended Internally Consistent Thermodynamic Dataset for Phases of Petrological Interest, Involving a New Equation of State for Solids." *Journal of Metamorphic Geology* 29, no. 3: 333–383. https://doi.org/10.1111/j.1525-1314.2010.00923.x.

Horton, B. K., and P. G. DeCelles. 1997. "The Modern Foreland Basin System Adjacent to the Central Andes." *Geology* 25, no. 10: 895–898. https://doi.org/10.1130/0091-7613(1997)025<0895:TMFBSA>2.3.CO;2.

Jackson, J., D. Mckenzie, K. Priestley, and B. Emmerson. 2008. "New Views on the Structure and Rheology of the Lithosphere." *Journal of the Geological Society* 165, no. 2: 453–465. https://doi.org/10.1144/0016-76492007-109.

Jackson, S. E., N. J. Pearson, W. L. Griffin, and E. A. Belousova. 2004. "The Application of Laser Ablation-Inductively Coupled Plasma-Mass Spectrometry to In Situ U-Pb Zircon Geochronology." *Chemical Geology* 211, no. 1: 47–69. https://doi.org/10.1016/j.chemgeo.2004.06.017.

Jackson, J., K. Priestley, M. Allen, and M. Berberian. 2002. "Active Tectonics of the South Caspian Basin." *Geophysical Journal International* 148, no. 2: 214–245. https://doi.org/10.1046/j.1365-246X.2002.01588.x.

Jaupart, C., J. C. Mareschal, L. Guillou-Frottier, and A. Davaille. 1998. "Heat Flow and Thickness of the Lithosphere in the Canadian Shield." *Journal of Geophysical Research: Solid Earth* 103, no. B7: 15269–15286. https://doi.org/10.1029/98JB01395.

Jochum, K. P., U. Weis, B. Stoll, et al. 2011. "Determination of Reference Values for NIST SRM 610-617 Glasses Following ISO Guidelines." *Geostandards and Geoanalytical Research* 35, no. 4: 397–429. https://doi.org/10.1111/j.1751-908X.2011.00120.x.

Jochum, K. P., M. Willbold, I. Raczek, B. Stoll, and K. Herwig. 2005. "Chemical Characterisation of the USGS Reference Glasses GSA-1G, GSC-1G, GSD-1G, GSE-1G, BCR-2G, BHVO-2G and BIR-1G Using EPMA, ID-TIMS, ID-ICP-MS and LA-ICP-MS." *Geostandards and Geoanalytical Research* 29, no. 3: 285–302. https://doi.org/10.1111/j.1751-908X.2005.tb00901.x.

Johnson, T. A., J. M. Cottle, and K. P. Larson. 2021. "Delineation of Multiple Metamorphic Events in the Himalayan Kathmandu Complex, Central Nepal." *Journal of Metamorphic Geology* 39, no. 4: 443–472. https://doi.org/10.1111/jmg.12583.

Johnstone, G. S., D. I. Smith, and A. L. Harris. 1969. "Moinian Assemblage of Scotland." edited by M. Kay, *North Atlantic-Geology and Continental Drift*, Vol. 12. American Association of Petroleum Geologists. https://doi.org/10.1306/M12367C13.

Kellett, D. A., O. M. Weller, A. Zagorevski, and D. Regis. 2018. "A Petrochronological Approach for the Detrital Record: Tracking mm-Sized Eclogite Clasts in the Northern Canadian Cordillera." *Earth and Planetary Science Letters* 494: 23–31. https://doi.org/10.1016/j.epsl.2018.04.036.

Kennedy, W. Q. 1949. "Zones of Progressive Regional Metamorphism in the Moine Schists of the Western Highlands of Scotland." *Geological Magazine* 86, no. 1: 43–56.

Kinnaird, T. C., A. R. Prave, C. L. Kirkland, M. S. A. Horstwood, R. R. Parrish, and R. A. Batchelor. 2007. "The Late Mesoproterozoic Early Neoproterozoic Tectonostratigraphic Evolution of NW Scotland: The Torridonian Revisited." *Journal of the Geological Society, London* 164: 541–551. https://doi.org/10.1144/0016-76492005-096.

Kirkland, C. L., R. A. Strachan, and A. R. Prave. 2008. "Detrital Zircon Signature of the Moine Supergroup, Scotland: Contrasts and Comparisons With Other Neoproterozoic Successions Within the Circum-North Atlantic Region." *Precambrian Research* 163, no. 3-4: 332–350. https://doi.org/10.1016/j.precamres.2008.01.003.

Kohn, M. J. 2020. "A Refined Zirconium-in-Rutile Thermometer." *American Mineralogist* 105, no. 6: 963–971. https://doi.org/10.2138/am-2020-7091.

Kooijman, E., M. A. Smit, K. Mezger, and J. Berndt. 2012. "Trace Element Systematics in Granulite Facies Rutile: Implications for Zr Geothermometry and Provenance Studies." *Journal of Metamorphic Geology* 30, no. 4: 397–412. https://doi.org/10.1111/j.1525-1314.2012.00972.x.

Korsman, K., T. Korja, M. Pajunen, P. Virransalo, and GGT/SVEKA Working Group. 1999. "The GGT/SVEKA Transect: Structure and Evolution of the Continental Crust in the Paleoproterozoic Svecofennian Orogen in Finland." *International Geology Review* 41, no. 4: 287–333. https://doi.org/10.1080/00206819909465144.

Krabbendam, M., H. Bonsor, M. S. A. Horstwood, and T. Rivers. 2017. "Tracking the Evolution of the Grenvillian Foreland Basin: Constraints From Sedimentology and Detrital Zircon and Rutile in the Sleat and Torridon Groups, Scotland." *Precambrian Research* 295: 67–89. https://doi.org/10.1016/j.precamres.2017.04.027.

Krabbendam, M., A. R. Prave, and D. Cheer. 2008. "A Fluvial Origin for the Neoproterozoic Morar Group, NW Scotland; Implications for Torridon-Morar Group Correlation and the Grenville Orogen Foreland Basin." *Journal of the Geological Society, London* 165: 379–394. https://doi.org/10.1144/0016-76492007-076.

Krabbendam, M., J. G. Ramsay, A. G. Leslie, P. W. G. Tanner, D. Dietrich, and K. M. Goodenough. 2018. "Caledonian and Knoydartian Overprinting of a Grenvillian Inlier and the Enclosing Morar Group Rocks: Structural Evolution of the Precambrian Proto-Moine Nappe, Glenelg, NW Scotland." *Scottish Journal of Geology* 54, no. 1: 13–35. https://doi.org/10.1144/sjg2017-006.

Krabbendam, M., R. Strachan, and T. Prave. 2022. "A New Stratigraphic Framework for the Early Neoproterozoic Successions of Scotland." *Journal of the Geological Society* 179, no. 2: jgs2021–054. https://doi.org/10.1144/jgs2021-054.

Lacombe, O., and F. Mouthereau. 2002. "Basement-Involved Shortening and Deep Detachment Tectonics in Forelands of Orogens: Insights From Recent Collision Belts (Taiwan, Western Alps, Pyrenees)." *Tectonics* 21, no. 4: 12–1–12–22. https://doi.org/10.1029/2001TC901018.

Lister, G., B. Kennett, S. Richards, and M. Forster. 2008. "Boudinage of a Stretching Slablet Implicated in Earthquakes Beneath the Hindu Kush." *Nature Geoscience* 1, no. 3: 196–201. https://doi.org/10.1038/ngeo132.

Ludwig, K. R. 1998. "On the Treatment of Concordant Uranium-Lead Ages." *Geochimica et Cosmochimica Acta* 62, no. 4: 665–676. https://doi.org/10.1016/S0016-7037(98)00059-3.

Luvizotto, G. L., and T. Zack. 2009. "Nb and Zr Behavior in Rutile During High-Grade Metamorphism and Retrogression: An Example From the Ivrea-Verbano Zone." *Chemical Geology* 261, no. 3: 303–317. https://doi.org/10.1016/j.chemgeo.2008.07.023.

Maggi, A., J. A. Jackson, D. McKenzie, and K. Priestley. 2000. "Earthquake Focal Depths, Effective Elastic Thickness, and the Strength of the Continental Lithosphere." *Geology* 28, no. 6: 495–498. https://doi.org/10.1130/0091-7613(2000)28<495:EFDEET>2.0.CO;2.

Manning, C. F., and S. R. Bohlen. 1991. "The Reaction Titanite+Kyanite=Anorthite+Rutile and Titanite-Rutile Barometry in Eclogites." *Contributions to Mineralogy and Petrology* 109, no. 1: 1–9. https://doi.org/10.1007/BF00687196.

Matenco, L. C., and B. U. Haq. 2020. "Multi-Scale Depositional Successions in Tectonic Settings." *Earth-Science Reviews* 200: 102991. https://doi.org/10.1016/j.earscirev.2019.102991.

May, F., J. Peacock, D. Smith, and A. Barber. 1993. *Geology of the Kintail District*. British Geological Survey.

Mazza, S. E., C. Mako, R. D. Law, M. J. Caddick, M. Krabbendam, and J. Cottle. 2018. "Thermobarometry of the Moine and Sgurr Beag Thrust Sheets, Northern Scotland." *Journal of Structural Geology* 113: 10–32. https://doi.org/10.1016/j.jsg.2018.05.002.

McDonough, W. F., and S. Sun. 1995. "The Composition of the Earth." *Chemical Geology* 120, no. 3: 223–253. https://doi.org/10.1016/0009-2541(94)00140-4.

McKenzie, D. 1978. "Some Remarks on the Development of Sedimentary Basins." *Earth and Planetary Science Letters* 40, no. 1: 25–32. https://doi.org/10.1016/0012-821X(78)90071-7.

McKenzie, D., J. Jackson, and K. Priestley. 2005. "Thermal Structure of Oceanic and Continental Lithosphere." *Earth and Planetary Science Letters* 233, no. 3: 337–349. https://doi.org/10.1016/j.epsl.2005.02.005.

McKenzie, D., W. Yi, and R. Rummel. 2015. "Estimates of $T_e$ for Continental Regions Using GOCE Gravity." *Earth and Planetary Science Letters* 428: 97–107. https://doi.org/10.1016/j.epsl.2015.07.036.

McMahon, W. J., and N. S. Davies. 2020. "Physical and Biological Functioning in Proterozoic Rivers: Evidence From the Archetypal Pre-Vegetation Alluvium of the Torridon Group, NW Scotland." *Scottish Journal of Geology* 56, no. 1: 1–29. https://doi.org/10.1144/sjg2019-013.

Mellors, R. J., J. Jackson, S. Myers, et al. 2012. "Deep Earthquakes Beneath the Northern Caucasus: Evidence of Active or Recent Subduction in Western Asia." *Bulletin of the Seismological Society of America* 102, no. 2: 862–866. https://doi.org/10.1785/0120110184.

Middleton, M. F. 1989. "A Model for the Formation of Intracratonic Sag Basins." *Geophysical Journal International* 99, no. 3: 665–676. https://doi.org/10.1111/j.1365-246X.1989.tb02049.x.

Mitra, S., K. Priestley, A. K. Bhattacharyya, and V. K. Gaur. 2005. "Crustal Structure and Earthquake Focal Depths Beneath Northeastern India and Southern Tibet." *Geophysical Journal International* 160, no. 1: 227–248. https://doi.org/10.1111/j.1365-246X.2004.02470.x.

Mitra, S., K. F. Priestley, K. Borah, and V. K. Gaur. 2018. "Crustal Structure and Evolution of the Eastern Himalayan Plate Boundary System, Northeast India." *Journal of Geophysical Research: Solid Earth* 123, no. 1: 621–640. https://doi.org/10.1002/2017JB014714.

Miyashiro, A. 1973. "Eclogites and the Eclogite Facies." edited by A. Miyashiro, *Metamorphism and Metamorphic Belts*. Dordrecht: Springer Netherlands, pp. 310–324. https://doi.org/10.1007/978-94-011-6836-6_15.

Najman, Y., L. Bracciali, R. R. Parrish, E. Chisty, and A. Copley. 2016. "Evolving strain Partitioning in the Eastern Himalaya: The Growth of the Shillong Plateau." *Earth and Planetary Science Letters* 433: 1–9. https://doi.org/10.1016/j.epsl.2015.10.017.

Nicholson, P. G. 1994. "A Basin Reappraisal of the Proterozoic Torridon Group, Northwest Scotland." In *Tectonic Controls and Signatures in*

*Sedimentary Successions*, pp. 183–202. https://doi.org/10.1002/9781444304053.ch11.

Olivar, J., S. Nacif, M. Gimenez, B. Heit, L. Fennell, and A. Folguera. 2023. "Structure and Seismogenic Activity of the Broken Foreland to the South of the Chilean-Pampean Flat Subduction Zone: The San Rafael Block." *Journal of South American Earth Sciences* 124: 104260. https://doi.org/10.1016/j.jsames.2023.104260.

Palin, R. M., G. S. Reuber, R. W. White, B. J. P. Kaus, and O. M. Weller. 2017. "Subduction Metamorphism in the Himalayan Ultrahigh-Pressure Tso Morari Massif: An Integrated Geodynamic and Petrological Modelling Approach." *Earth and Planetary Science Letters* 467: 108–119. https://doi.org/10.1016/j.epsl.2017.03.029.

Park, R. G. 1995. "Palaeoproterozoic Laurentia-Baltica Relationships: A View From the Lewisian." *Geological Society, London, Special Publications* 95, no. 1: 211–224. https://doi.org/10.1144/GSL.SP.1995.095.01.13.

Park, G. 2022. "A Regional Explanation for Laxfordian Tectonic Evolution and Its Implications for the Lewisian Terrane Model." *Scottish Journal of Geology* 58, no. 1: sjg2021–020. https://doi.org/10.1144/sjg2021-020.

Patchett, P. J., G. Bylund, and B. G. J. Upton. 1978. "Palaeomagnetism and the Grenville Orogeny: New Rb-Sr Ages From Dolerites in Canada and Greenland." *Earth and Planetary Science Letters* 40, no. 3: 349–364. https://doi.org/10.1016/0012-821X(78)90159-0.

Peach, B. N., J. Horne, W. Gunn, C. T. Clough, L. W. Hinxman, and J. J. H. Teall. 1907. *The Geological Structure of the North-West Highlands of Scotland*. Geological Survey Her Majesty's Stationery Office.

Peach, B. N., H. Woodward, C. Clough, A. Harker, and C. Wedd. 1910. *The Geology of Glenelg, Lochalsh and South East Part of Skye*, Memoirs of the Geological Survey of Great Britain. Edinburgh: HMSO.

Peterman, E. M., B. R. Hacker, and E. F. Baxter. 2009. "Phase Transformations of Continental Crust During Subduction and Exhumation: Western Gneiss Region, Norway." *European Journal of Mineralogy* 21, no. 6: 1097–1118. https://doi.org/10.1127/0935-1221/2009/0021-1988.

Peters, D. 2001. "Geochemical and Geochronological Assessment of the Great Glen Fault as a Terrane Boundary." (PhD thesis), Keele University.

Podugu, N., L. Ray, S. P. Singh, and S. Roy. 2017. "Heat Flow, Heat Production, and Crustal Temperatures in the Archaean Bundelkhand Craton, North-Central India: Implications for Thermal Regime Beneath the Indian Shield." *Journal of Geophysical Research: Solid Earth* 122, no. 7: 5766–5788. https://doi.org/10.1002/2017JB014041.

Rainbird, R. H., M. A. Hamilton, and G. M. Young. 2001. "A Fluvial Origin for the Neoproterozoic Morar Group, NW Scotland; Implications for Torridon-Morar Group Correlation and the Grenville Orogen Foreland Basin." *Journal of the Geological Society, London* 2001: 15–27. https://doi.org/10.1144/0016-76492007-076.

Rainbird, R. H., N. M. Rayner, T. Hadlari, et al. 2017. "Zircon Provenance Data Record the Lateral Extent of Pancontinental, Early Neoproterozoic Rivers and Erosional Unroofing History of the Grenville Orogen." *GSA Bulletin* 129: 1408–1423. https://doi.org/10.1130/b31695.1.

Ramsay, J. G. 1957. "Moine-Lewisian Relations at Glenelg, Inverness-Shire." *Quarterly Journal of the Geological Society, London* 113: 487–520. https://doi.org/10.1144/GSL.JGS.1957.113.01-04.21.

Rawson, J. R., D. A. Carswell, and D. Smallwood. 2001. "Garnet-Bearing Olivine-Websterite Within the Eastern Glenelg Lewisian of the Glenelg Inlier, NW Highlands." *Scottish Journal of Geology* 37, no. 1: 27–34. https://doi.org/10.1144/sjg37010027.

Rivers, T. 1997. "Lithotectonic Elements of the Grenville Province: Review and Tectonic Implications." *Precambrian Research* 86, no. 3: 117–154. https://doi.org/10.1016/S0301-9268(97)00038-7.

Rivers, T., N. Culshaw, A. Hynes, A. Indares, R. Jamieson, and J. Martignole. 2012. "The Grenville Orogen - A Post-LITHOPROBE Perspective." edited by K. A. Percival, F. A. Cook, and R. M. Clowes, *Tectonic Styles in Canada*, Vol. 49. Geological Association of Canada, pp. 97–236.

Roberts, A. M., R. A. Strachan, A. L. Harris, D. Barr, and R. E. Holdsworth. 1987. "The Sgurr Beag Nappe: A Reassessment of the Stratigraphy and Structure of the Northern Highland Moine." *GSA Bulletin* 98, no. 5: 497–506. https://doi.org/10.1130/0016-7606(1987)98<497:TSBNAR>2.0.CO;2.

Rogers, G., P. D. Kinny, R. A. Strachan, C. R. L. Friend, and B. A. Paterson. 2001. "U-Pb Geochronology of the Fort Augustus Granite Gneiss: Constraints on the Timing of Neoproterozoic and Palaeozoic Tectonothermal Events in the NW Highlands of Scotland." *Journal of the Geological Society* 158, no. 1: 7–14. https://doi.org/10.1144/jgs.158.1.7.

Rudnick, R. L., and D. M. Fountain. 1995. "Nature and Composition of the Continental Crust: A Lower Crustal Perspective." *Reviews of Geophysics* 33, no. 3: 267–309. https://doi.org/10.1029/95RG01302.

Sajeev, K., T. Kawai, S. Omori, B. F. Windley, and S. Maruyama. 2010. "P-T Evolution of Glenelg Eclogites, NW Scotland: Did They Experience Ultrahigh-Pressure Metamorphism?." *Lithos* 114, no. 3-4: 473–489. https://doi.org/10.1016/j.lithos.2009.10.007.

Salminen, J., S. A. A. Elming, and P. Layer. 2023. "Timing the Break-Up of the Baltica and Laurentia Connection in Nuna – Rapid Plate Motion Oscillation and Plate Tectonics in the Mesoproterozoic." *Precambrian Research* 384: 106923. https://doi.org/10.1016/j.precamres.2022.106923.

Sanders, I. S. 1988. "Plagioclase Breakdown and Regeneration Reactions in Grenville Kyanite Eclogite at Glenelg, NW Scotland." *Contributions to Mineralogy and Petrology* 98: 33–39. https://doi.org/10.1007/BF00371907.

Sanders, I. S., P. van Calsteren, and C. Hawkesworth. 1984. "A Grenville Sm-Nd Age for the Glenelg Eclogite in Northwest Scotland." *Nature* 312: 439–440. https://doi.org/10.1038/312439a0.

Santos, M. M., C. Lana, R. Scholz, et al. 2017. "A New Appraisal of Sri Lankan BB Zircon as a Reference Material for LA-ICP-MS U-Pb Geochronology and Lu-Hf Isotope Tracing." *Geostandards and Geoanalytical Research* 41, no. 3: 335–358. https://doi.org/10.1111/ggr.12167.

Schmitt, A. K., and T. Zack. 2012. "High-Sensitivity U-Pb Rutile Dating by Secondary Ion Mass Spectrometry (SIMS) With an $O^{2+}$ Primary Beam." *Chemical Geology* 332-333: 65–73. https://doi.org/10.1016/j.chemgeo.2012.09.023.

Searle, M. P. 2022. "Tectonic Evolution of the Caledonian Orogeny in Scotland: A Review Based on the Timing of Magmatism, Metamorphism and Deformation." *Geological Magazine* 159, no. 1: 124–152. https://doi.org/10.1017/S0016756821000947.

Sláma, J., J. Košler, D. J. Condon, et al. 2008. "Plešovice Zircon– A New Natural Reference Material for U–Pb and Hf Isotopic Microanalysis." *Chemical Geology* 249, no. 1: 1–35. https://doi.org/10.1016/j.chemgeo.2007.11.005.

Smithson, S. B., J. A. Brewer, S. Kaufman, J. E. Oliver, and C. A. Hurich. 1979. "Structure of the Laramide Wind River Uplift, Wyoming, From COCORP Deep Reflection Data and From Gravity Data." *Journal of Geophysical Research: Solid Earth* 84, no. B11: 5955–5972. https://doi.org/10.1029/JB084iB11p05955.

Soper, N. J., and P. E. Brown. 1972. "Relationship Between Metamorphism and Migmatization in the Northern Part of the Moine Nappe." *Scottish Journal of Geology* 7, no. 4: 305–325. https://doi.org/10.1144/sjg07040305.

Soper, N. J., A. L. Harris, and R. A. Strachan. 1998. "Tectonostratigraphy of the Moine Supergroup: A Synthesis." *Journal of the Geological Society* 155, no. 1: 13–24. https://doi.org/10.1144/gsjgs.155.1.0013.

Spear, F. S., D. R. M. Pattison, and J. T. Cheney. 2017. "The metamorphosis of Metamorphic Petrology." *The Web of Geological Sciences:*

*Advances, Impacts, and Interactions II*, Vol. 523. Geological Society of America. https://doi.org/10.1130/2016.2523(02).

Spencer, C., C. Kirkland, and R. Taylor. 2016. "Strategies Towards Statistically Robust Interpretations of In Situ U-Pb Zircon geochronology." *Geoscience Frontiers* 7, no. 4: 581–589. https://doi.org/10.1016/j.gsf.2015.11.006.

Stewart, A. D. 1969. "Torridonian Rocks of Scotland Reviewed: Northwestern Border of the Orogenic Belt." *North Atlantic: Geology and Continental Drift*, Memoir. American Association of Petroleum Geologists.

Stewart, A. D. 2002. *The Later Proterozoic Torridonian Rocks of Scotland: Their Sedimentology, Geochemistry and Origin*. Geological Society of London. https://doi.org/10.1144/GSL.MEM.2002.024.

Storey, C. D. 2002. "Tectono-Metamorphic Evolution of the Glenelg-Attadale Inlier, Northwest Scotland." (PhD thesis), University of Leicester (United Kingdom).

Storey, C. D. 2008. "The Glenelg-Attadale Inlier, NW Scotland, With Emphasis on the Precambrian High-Pressure Metamorphic History and Subsequent Retrogression: an introduction and review." *Scottish Journal of Geology* 44, no. 1: 1–16. https://doi.org/10.1144/sjg44010001.

Storey, C. D., T. S. Brewer, R. Anczkiewicz, R. R. Parrish, and M. F. Thirlwall. 2010. "Multiple High-Pressure Metamorphic Events and Crustal Telescoping in the NW Highlands of Scotland." *Journal of the Geological Society* 167, no. 3: 455–468. https://doi.org/10.1144/0016-76492009-024.

Storey, C. D., T. S. Brewer, and R. R. Parrish. 2004. "Late-Proterozoic Tectonics in Northwest Scotland: One Contractional Orogeny or Several?." *Precambrian Research* 134, no. 3: 227–247. https://doi.org/10.1016/j.precamres.2004.06.004.

Storey, C. D., T. S. Brewer, and S. Temperley. 2005. "P-T Conditions of Grenville-Age Eclogite Facies Metamorphism and Amphibolite Facies Retrogression of the Glenelg-Attadale Inlier, NW Scotland." *Geological Magazine* 142, no. 5: 605–615. https://doi.org/10.1017/s001675680500110x.

Strachan, R. A. 1985. "The Stratigraphy and Structure of the Moine Rocks of the Loch Eil Area, West Inverness-Shire." *Scottish Journal of Geology* 21, no. 1: 9–22. https://doi.org/10.1144/sjg21010009.

Strachan, R. A. 1986. "Shallow Marine Sedimentation in the Proterozoic Moine Succession, Northern Scotland." *Precambrian Research* 32, no. 1: 17–33. https://doi.org/10.1016/0301-9268(86)90027-6.

Strachan, R. A., T. E. Johnson, C. L. Kirkland, P. D. Kinny, and T. Kusky. 2020. "A Baltic Heritage in Scotland: Basement Terrane Transfer During the Grenvillian Orogeny." *Geology* 48, no. 11: 1094–1098. https://doi.org/10.1130/g47615.1.

Sutton, J., and J. Watson. 1958. "Structures in the Caledonides Between Loch Duich and Glenelg, Northwest Highlands." *Quarterly Journal of the Geological Society, London* 114: 231–255. https://doi.org/10.1144/gsjgs.114.1.0231.

Sutton, J., and J. Watson. 1964. "Some Aspects of Torridonian Stratigraphy in Skye." *Proceedings of the Geologists' Association* 75, no. 3: 251–IN1. https://doi.org/10.1016/S0016-7878(64)80033-X.

Tanner, P. W. G. 1971. "The Sgurr Beag Slide – A Major Tectonic Break Within the Moinian of the Western Highlands of Scotland." *Quarterly Journal of the Geological Society of London* 126, no. 1-4: 435–463. https://doi.org/10.1144/gsjgs.126.1.0435.

Thigpen, J. R., R. D. Law, C. L. Loehn, et al. 2013. "Thermal Structure and Tectonic Evolution of the Scandian Orogenic Wedge, Scottish Caledonides: Integrating Geothermometry, Deformation Temperatures and Conceptual Kinematic-Thermal Models." *Journal of Metamorphic Geology* 31, no. 8: 813–842. https://doi.org/10.1111/jmg.12046.

Turnbull, M. J. M., M. J. Whitehouse, and S. Moorbath. 1996. "New isotopic Age Determinations for the Torridonian, NW Scotland." *Journal of the Geological Society* 153, no. 6: 955–964. https://doi.org/10.1144/gsjgs.153.6.0955.

Vermeesch, P. 2018. "IsoplotR: A Free and Open Toolbox for Geochronology." *Geoscience Frontiers* 9, no. 5: 1479–1493. https://doi.org/10.1016/j.gsf.2018.04.001.

Weller, O. M., C. M. Mottram, M. R. St-Onge, et al. 2021. "The Metamorphic and Magmatic Record of Collisional Orogens." *Nature Reviews Earth and Environment* 2, no. 11: 781–799. https://doi.org/10.1038/s43017-021-00218-z.

Wheeler, J., R. G. Park, H. R. Rollinson, and A. Beach. 2010. "The Lewisian Complex: Insights Into Deep Crustal Evolution." *Geological Society, London, Special Publications* 335, no. 1: 51–79. https://doi.org/10.1144/SP335.4.

White, R. W., R. Powell, T. J. B. Holland, T. E. Johnson, and E. C. R. Green. 2014. "New Mineral Activity-Composition Relations for Thermodynamic Calculations in Metapelitic Systems." *Journal of Metamorphic Geology* 32, no. 3: 261–286. https://doi.org/10.1111/jmg.12071.

Whitney, D. L., and B. W. Evans. 2010. "Abbreviations for Names of Rock-Forming Minerals." *American Mineralogist* 95, no. 185-187. https://doi.org/10.2138/am.2010.3371.

Wiedenbeck, M., P. Alle, F. Corfu, et al. 1995. "Three Natural Zircon Standards for U-Th-Pb, Lu-Hf, Trace Element and REE Analyses." *Geostandards Newsletter* 19, no. 1: 1–23. https://doi.org/10.1111/j.1751-908X.1995.tb00147.x.

Williams, G. E., and J. Foden. 2011. "A Unifying Model for the Torridon Group (Early Neoproterozoic), NW Scotland: Product of Post-Grenvillian Extensional Collapse." *Earth-Science Reviews* 108, no. 1: 34–49. https://doi.org/10.1016/j.earscirev.2011.05.004.

Wimpenny, S. 2022. "Weak, Seismogenic Faults Inherited From Mesozoic Rifts Control Mountain Building in the Andean Foreland." *Geochemistry, Geophysics, Geosystems* 23, no. 3: e2021GC010270. https://doi.org/10.1029/2021GC010270.

Yin, A. 2006. "Cenozoic Tectonic Evolution of the Himalayan Orogen as Constrained by Along-Strike Variation of Structural Geometry, Exhumation History, and Foreland Sedimentation." *Earth-Science Reviews* 76, no. 1: 1–131. https://doi.org/10.1016/j.earscirev.2005.05.004.

Zack, T., D. F. Stockli, G. L. Luvizotto, et al. 2011. "In Situ U-Pb Rutile Dating by LA-ICP-MS: 208Pb Correction and Prospects for Geological Applications." *Contributions to Mineralogy and Petrology* 162, no. 3: 515–530. https://doi.org/10.1007/s00410-011-0609-4.

Zhang, G., L. Zhang, A. G. Christy, S. Song, and Q. Li. 2014. "Differential Exhumation and Cooling History of North Qaidam UHP Metamorphic Rocks, NW China: Constraints From Zircon and rutile thermometry and U-Pb geochronology." *Lithos* 205: 15–27. https://doi.org/10.1016/j.lithos.2014.06.018.

Zhao, Z.-F., Y.-F. Zheng, R.-X. Chen, Q.-X. Xia, and Y.-B. Wu. 2007. "Element Mobility in Mafic and Felsic Ultrahigh-Pressure Metamorphic Rocks During Continental Collision." *Geochimica et Cosmochimica Acta* 71, no. 21: 5244–5266. https://doi.org/10.1016/j.gca.2007.09.009.

Zheng, D., S. Wu, C. Ma, et al. 2022. "Zircon Classification From Cathodoluminescence Images Using Deep Learning." *Geoscience Frontiers* 13, no. 6: 101436. https://doi.org/10.1016/j.gsf.2022.101436.

## Supporting Information

Additional supporting information can be found online in the Supporting Information section.